Terfenol Based Optical Phase Modulator and Magnetometer

by
Ketan Dilip Kamdar

Thesis submitted to the Faculty of the
Virginia Polytechnic Institute and State University
in partial fulfillment of the requirements for the degree of

MASTER OF SCIENCE
in
Electrical Engineering

APPROVED:

Richard O. Claus, Chairman

Ira Jacobs

Kent Murphy

May, 1993
Blacksburg, Virginia

Terfenol Based Optical Phase Modulator and Magnetometer

by

Ketan Dilip Kamdar

Richard O. Claus, Chairman
Electrical Engineering

Two new fiber optic magnetostrictive phase modulators and magnetometers using the highly magnetostrictive rare-earth iron compound $Tb_xDy_{1-x}Fe_2$ are investigated. They demonstrated to have a high sensitivity, dynamic range, minimum field detectability, and a better structural suitability than metallic glasses. For the first sensor, the experimental linear phase shifting coefficient was 1.102 rad/Vp-m with the corresponding phase shift normalized to the magnetic field of 0.306 rad/G-m. For the second sensor, the experimental linear phase shifting coefficient was 0.5 rad/Vp-m with the corresponding phase shift normalized to the magnetic field of 0.136 rad/G-m. A minimum detectable phase shift of better than 1 μrad was obtained, which corresponds to 2 μG/m for a 4 Hz bandwidth and 1 $\mu G/\sqrt{Hz}$ per meter of fiber interaction length. The projected minimum detectable magnetic field for 30 meters, for the first sensor, is thus seen to be $3pT/\sqrt{Hz}$. The experimental results presented have clearly demonstrated the utility of the Terfenol based magnetostrictive fiber optic phase modulator and magnetometer.

Acknowledgments

I would like to thank a number of people, for without their help, this work might never have been possible. First of all I would like to thank Dr. Richard O. Claus for giving me the opportunity to work at FEORC and explore the fascinating world of fiber optics. His constant encouragement and positive attitude helped me get through the dark moments of my research. I would also like to thank Dr. Ira Jacobs and Dr. Kent Murphy for their useful discussions and help and for serving on my committee.

I am grateful to Dr. V. S. Sudarshanam for helping and guiding me through every step on the way. I also wish to thank Mike Gunther, Russell May, Anbo Wang, and Marten DeVries for their valuable suggestions and assistance. A special thanks to Linda Jones and the other members of FEORC for making this experience a pleasure.

Finally, I am deeply grateful for the love and support extended to me by my family, especially my parents, Dilip Kamdar and Dipti Kamdar, and my uncles Prabhakar Kamdar and Vinoo Kamdar and my aunt Bharati Bhayani. Above all, I wish to thank my girlfriend and now fiancé, Shilpa, for her love and understanding during the long hours and for giving me the courage to try to be the best that I can be.

Table of Contents

List of Figures

List of Tables

Chapter 1 - Introduction

1.1 Background

Since the beginning of this century, communication system carrier frequencies have increased in magnitude dramatically. Optical frequencies offered very high bandwidth and with the development of laser technology, many free space transmission systems were proposed and tested in the 1960s. With the introduction of very low loss fused silica glass, communication system design shifted focus from free space to fiber based systems. In a span of 25 years, optical fiber based communication systems evolved from a lab curiosity to a powerful, practical, and widely used communication technology [1.1].

Optical fiber seems to be an almost ideal communication channel because it has a very large bandwidth and has a high degree of isolation from surrounding environmental perturbations. Crosstalk, or coupling of energy between fibers, becomes insignificant because the evanescent fields in the outermost part of the cladding decay to negligible levels. Optical fiber exhibits a low sensitivity to incident electromagnetic fields because it is fabricated from dielectric materials. Also, maintaining and upgrading existing fiber

systems is more easily accomplished because optical fibers are significantly smaller than traditional electrical cables per unit bandwidth. Thus, optical fiber, with these inherent characteristics revolutionized telecommunications. With technical improvements and development of optoelectronic components another revolution began as designers combined the product outgrowth of these two areas to create fiber optic sensors. The areas of opportunity are staggering and include the potential of replacing the majority of environmental sensors in existence today as well as opening up entire markets where sensors with comparable capability do not exist. The following sections describe how the optical fiber can be made highly sensitive to environmental perturbations.

1.2 Optical Fibers for Sensing Applications

Fiber optic sensors are today finding applications in nondestructive testing (NDT) of materials and structures. Structural engineers envision a "smart structure" in which they desire to incorporate sensing, decision making, and actuating mechanisms into inherently flexible structures. This could be accomplished by embedding within the protective skin of the structure, a fiber network with multiplexed sensors sensitive to different perturbations which need to be monitored, thus giving "nerves" to a structure. Magnetic, acoustic, pressure, temperature, displacement, acceleration, gyro, torque, current, fluid level, photo acoustic, and strain are among the fiber optic sensor types being investigated.

Fiber sensors offer a number of advantages:

- increased sensitivity over existing techniques,
- geometric versatility in that fiber sensors can be configured in arbitrary shapes,

- dielectric (passive) construction so that they can be used in high voltage, high temperature, electrically noisy, corrosive, or other stressing environments,
- light weight,
- small size,
- large bandwidth, and
- electrical and optical multiplexing capability.

With these attributes and its inherent compatibility with optical fiber telemetry technology, fiber optic sensors offer unparalleled flexibility.

The sensors can be constructed either intrinsically or extrinsically. Intrinsic sensors rely on external perturbations directly affecting the light traveling within the optical waveguide. Extrinsic sensors are distinguished by the characteristic that sensing takes place in a region outside the fiber. For example, mode coupling due to strain in elliptical core fibers is an intrinsic effect and alignment losses between two fiber endfaces is an extrinsic effect.

Fiber optic sensors are further classified, based on two basic sensing schemes, into amplitude sensors or phase (interferometric) sensors. In the first case, the physical perturbation interacts with the fiber or some device attached to the fiber to directly modulate the intensity of light in the fiber. Interferometric sensors rely on some perturbation modulating the phase of the light propagating in the fiber. The advantage of intensity based systems is the simplicity of construction and implementation because of the simplistic modulation techniques. Also, single mode and multimode fibers can be used. The most prevalent limitation of intensity based sensors is that they are generally less sensitive than their interferometric counterparts. However, since extreme sensitivity is not

required for most applications and the fact that these devices are competitive with existing devices, a large market appears to exist for this class of sensors.

Interferometric sensors, as mentioned above, are based upon monitoring the phase of light propagating in an optical fiber. Thus, a known reference signal is required to accurately monitor the phase of light. To accomplish this, these sensors are usually constructed with two separate optical fibers, or arms, with one arm ideally uninfluenced by the environment, called the reference arm, and the other influenced by the environment, called the sensing arm. Light propagating through the two separate arms is combined together, and the resulting output intensity becomes a function of the interference between the two optical waves. When the signals are exactly in phase, then the output intensity is a maximum, and when the signals are exactly out of phase, the output intensity is a minimum. It should be noted that to have interference of only two waves, the fiber used in the two arms should be singlemode fiber. Practical implementations of this design include the Mach Zehnder and Michelson interferometers.

Interferometric sensors have certain disadvantages associated with them. Lasers used with optical fibers have operating wavelengths in the range of 600 nm to 1500 nm. Any fluctuations associated with the laser will affect the optical path length and thus add false phase information to the detected signal. Also, mechanical motions of the fiber caused by air currents, and temperature changes also affect the performance. Thus, extreme care must be taken to insure that none of these effects affect the sensitivity of the sensor by coupling extraneous phase information into the sensor response.

1.3 Introduction to Magnetic Field Sensors and Phase Modulators

Of the several physical parameters that optical fibers can be made sensitive to, magnetic field strength forms a significant quantity of interest for detection. There exists a need for magnetic field detection in certain applications of smart structures involving magnetic means of actuation. Also, most of the fiber sensor systems involve to a specific sophistication some detection scheme which requires the use of phase modulators. Fiber optic phase modulation through the magnetostriction of certain materials to which the fiber is bonded forms a common method of generation and detection of signals. Several designs of fiber optic magnetostrictive phase modulators [1.2] and magnetometers [1.3, 1.4, 1.5, 1.6] have been demonstrated after the first proposal and analysis, in 1979, of a fiber sensor with a magnetostrictive jacket.

Five distinct technologies have been developed [1.7] for magnetic field sensors for the measurement of low-frequency (< 10 Hz) magnetic fields at levels below 10^{-9} T,

- fluxgates,
- precession devices,
- superconducting quantum interference devices (SQUIDS),
- fiber optic devices, and
- stress driven magnetoelastic devices.

For the measurement of high frequency (>10 Hz) magnetic fields, it is difficult to surpass the performance and simplicity of a sensor made from a coil of wire and a preamplifier. But a nonconducting probe is advantageous in the presence of electromagnetic

interference or high voltage environments. For high frequency magnetic sensing, the devices available are:

- wire loop (search coil),
- bulk optic Faraday devices, and
- fiber optic devices.

For the measurement of magnetic fields, two basic approaches exist. The first is the Faraday rotation approach and the second is the magnetostrictive or stretcher approach. Faraday discovered that circular birefringence can be induced in a variety of materials by the application of a magnetic field. Therefore, it is possible to sense magnetic fields by using linearly polarized light to measure the amount of circular birefringence, induced by an external magnetic field in certain materials.

However, only large currents and magnetic fields can be detected by the Faraday approach, since the Verdet constant of most silica doped fibers is small [1.6, 1.7]. Rare earth ions can be doped into silica to enhance the Faraday effect. However, the optical absorption introduced by the ions and constraints on solubility of the ion in silica limit the practical realization. It requires sophisticated fiber drawing techniques and special materials to provide highly sensitive detection of magnetic fields.

The second approach, using magnetostrictive materials has a potential of much greater sensitivity and is more straightforward. The transducers developed using this approach can be used as magnetic field sensors and phase modulators. The primary issue to be solved using magnetostrictive materials is the identification of such materials and the incorporation of such materials into a fiber sensor by appropriate bonding or coating. This

is the motivation behind this thesis. The next chapter explains the principles of magnetostrictive sensors and presents the results obtained with metallic glass sensors. Chapter 3, investigates the properties of rare earth iron compounds and the properties of Terfenol. Chapter 4 explains the basics of two beam interferometry and the detection scheme employed. It then explains the experimental setup, sensor designs and discusses the results. Chapter 5 is the conclusion and looks into the possible directions in which this research can evolve.

Chapter 2 - Principles of Magnetostrictive Transducers

2.1 Introduction

Of the several physical parameters that optical fibers can be made sensitive to, magnetic field strength forms a significant quantity of interest for detection. There exists a need for magnetic field detection in certain applications of smart structures involving magnetic means of actuation. Also, most of the fiber sensor systems use some sophisticated detection scheme which requires the use of phase modulators. Fiber optic phase modulation through the magnetostriction of certain materials to which the fiber is bonded forms a common method of generation and detection of signals. Several designs of fiber optic magnetostrictive phase modulators [1.2] and magnetometers [1.3, 1.4, 1.5, 1.6] have been demonstrated after the first proposal and analysis, in 1979, of a fiber sensor with a magnetostrictive jacket.

Magnetostriction is described as a change in dimension of a ferromagnetic material when it is placed along the axis of an applied magnetic field. Magnetostrictive fiber optic sensors

employ a fiber interferometer to measure the magnetic field-dependent strain in a transducing material. A basic Mach Zehnder interferometer configuration consisting of a magnetostrictive material bonded to a fiber of length L in one arm of the interferometer is shown in Figure 2.1. A detailed introduction to the principles of the Mach Zehnder interferometer is explained in Chapter 4.

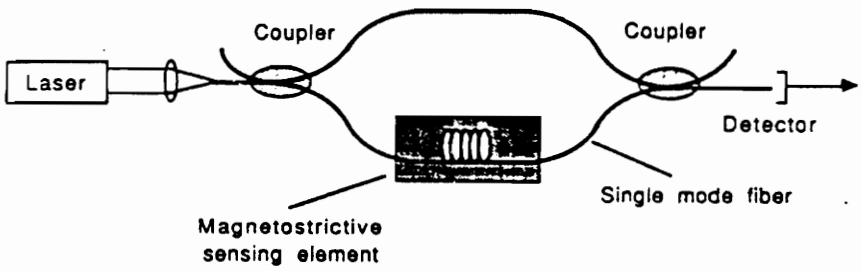

Figure 2.1. Basic components of a magnetostrictive fiber optic sensor using a Mach Zehnder interferometer [1.7].

If the strain 'e' of the material depends on the externally applied magnetic field H, the field dependent phase shift $\phi(H)$ induced in the interferometer is given by

$$\phi(H) = \frac{2\pi n \xi}{\lambda} L \eta e(H) \tag{2.1}$$

where n is the refractive index of the fiber core, L is the length of fiber undergoing field-dependent strain e(H), λ is the free space wavelength of the laser source, η the strain transfer efficiency (strain in fiber/strain in magnetostrictive material) and ξ is the strain optic correction factor, which accounts for the change in propagation constant with axial strain in the fiber core [2.1, 1.7],

$$\xi = 1 - \frac{1}{2} n^2 \left[(1-\mu) P_{12} - \mu P_{11} \right] \tag{2.2}$$

where μ is Poisson's ratio for the fiber material and P_{ij} are the elements of the strain optic sensor. For silica fiber n=1.46 and ξ is approximately 0.78, giving $n\xi$ = 1.14. Losses always occur in the interface between the fiber and the material. Therefore, all the strain developed by the magnetostrictive element is not transferred to the core of the fiber. The amount of strain transferred depends on the type and thickness of the adhesive used to bond the fiber to the magnetostrictive material, the dither frequency, and the type of fiber jacketing material. For jacketed single-mode fiber and epoxy adhesives, experimental values lie in the range $0.3<\eta<0.9$.

2.2 Magnetostriction

The magnetostriction for most ferromagnetic materials can be written as

$$e = CH^2 \tag{2.3}$$

where H is the total magnetic field and C is the magnetostriction parameter. Equation 2.3 describes the 'coherent rotation model', valid only under the set of conditions illustrated in Figure 2.2.

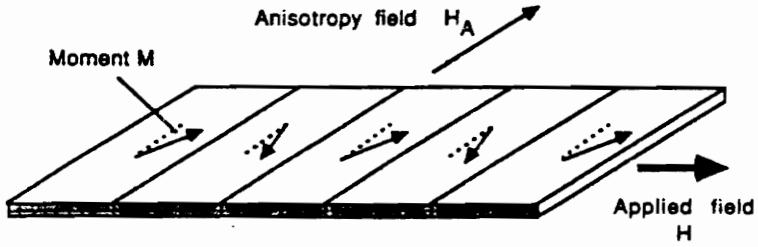

Figure 2.2. Domain structure in a transversely annealed metallic glass sample. The response of the moments to applied fields follows the coherent rotation model [1.7].

The model assumes that the material possesses uniaxial magnetic anisotropy defining an easy axis characterized by an anisotropy field H_A. This anisotropy results from two factors. The local atomic configuration in the vicinity of the moment, called crystalline anisotropy and the macroscopic shape of the sample called shape anisotropy. The magnetostatic energy of the sample as a whole, is minimized by a domain structure which shows an easy axis in the plane of the ribbon and perpendicular to the direction of the applied field. When a magnetic field is applied, the moments rotate coherently towards the direction of the field. The magnetization increases linearly with the applied field causing a

change in the length of the sample along the direction of the field which depends quadratically on the applied field as given in Equation 2.3.

The strain asymptotically approaches the saturation magnetostriction λ_S, when the magnitude of the applied field increases beyond H_A. C, the magnetostriction parameter, depends on λ_S and H_A according to the relation [1.7]

$$C = \frac{3\lambda_s}{2H_A^2}. \tag{2.4}$$

Thus, a material should have both a large λ_S and a small H_A to be useful for magnetostrictive sensor applications. The materials studied in depth so far are nickel and amorphous ferromagnetic metallic glass alloys. This thesis investigates a new material whose characteristics are described in the next chapter.

Annealing the material near its Curie temperature in the presence of a field has relatively little effect on λ_S, but can significantly reduce H_A, resulting in an increase in C. The C parameter can be increased by approximately a factor of 10, typically from 10^{-7} Oe^{-2} to 10^{-6} Oe^{-2}. It should be noted that the coherent rotation model is an equilibrium model since it was derived from minimization of a thermodynamic potential. It is important to understand the dynamic magnetostrictive response of the sample for magnetic sensors in which dithering is used. The nonlinear dependence of the magnetostriction on H is the most significant feature of Equation 2.3. For the measurement of low frequency magnitude fields this property is particularly important.

Consider a magnetic field 'H' given as:

$$H = H_0 + H_\omega \cos \Omega t + h \cos \omega t \tag{2.5}$$

where H_0 is a dc component, there is a slowly varying component at frequency Ω and a high frequency component at ω ($\omega >> \Omega$). On applying this field to the magnetostrictive element, the phase shift will consist of frequency components at the sum and difference frequencies $\omega \pm \Omega$, a dc component and components at Ω, 2Ω, ω and 2ω. To measure the dc and low frequency fields, under the assumption that the high frequency field can be controlled, it is sufficient to measure only the phase shifted components at ω and $\omega \pm \Omega$ having amplitudes

$$\phi_w(H_0) = \left(2\frac{2\pi n\xi}{\lambda} CLh\right) H_0 \tag{2.6}$$

$$\phi_{w\pm\Omega}(H_\Omega) = \left(\frac{2\pi n\xi}{\lambda} CLh\right) H_\Omega \tag{2.7}$$

Thus the amplitude of the component at ω varies linearly with H_0, for a fixed h, and the amplitude of the sidebands at $\omega \pm \Omega$ varies linearly with the low-frequency field amplitude H_Ω. The high frequency magnetic field is called the dither field or modulation field or magnetic carrier.

The interferometer phase noise power exhibits a 1/f frequency dependence. At frequencies above 1 kHz the rms phase noise of a well constructed fiber interferometer can easily be in the range of 1 to 10 $\mu rad/\sqrt{Hz}$. Thus a desirable operating condition for a

fiber optic sensor is one in which the limit to detection of a signal at frequency ω is the intrinsic phase noise of the interferometer.

2.3 Transducer Designs

Four basic transducer designs are shown in Figure 2.3:

(a) fiber with a magnetostrictive jacket

(b) fiber bonded to an amorphous alloy wire

(c) a bulk magnetostrictive cylinder or mandrel with fiber bonded to its circumference

(d) fiber bonded to a rectangular metallic strip.

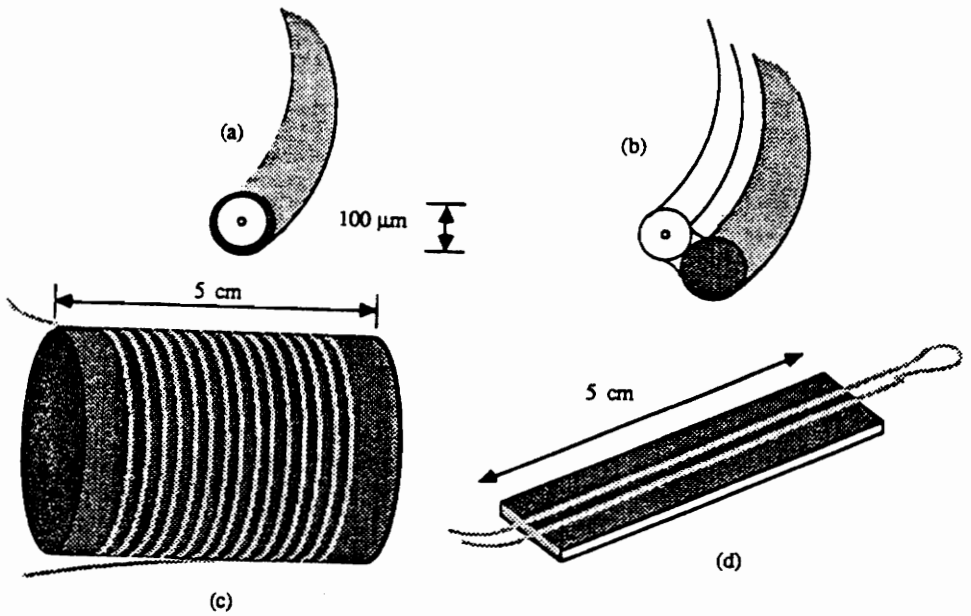

Figure 2.3: Transducer Designs [2.15]

Before evaluating these transducer designs, it is necessary to understand the following three effects.

Demagnetization:

In a highly permeable material, the magnetic moments in the sample respond to the applied field in such a way that if the material has positive magnetic susceptibility, the moments respond in a manner that partially cancels the externally applied field. Thus, the magnetic field inside a highly permeable material is never equal to the externally applied field [1.7]. The internal and external fields, considering only one direction, are related by:

$$H_{\text{int}} = \frac{H_{ext}}{1+N\chi} \tag{2.8}$$

where N is the demagnetization factor and χ is the volume magnetic susceptibility. N depends only on the geometry of the sample and χ relates the magnetization M to the internal field strength, given by

$$M = \chi H_{\text{int}} \tag{2.9}$$

A rough approximation assuming dc fields and neglecting edge effects can be made when the ratio of the area A_m of the sample perpendicular to the field is small compared to the square of the length L_m of the sample parallel to the field, and is given by [1.7]

$$N \approx \frac{8A_m}{L_m^2} \tag{2.10}$$

Mechanical Loading:

When a non magnetostrictive material, such as a fiber, is bonded to a magnetostrictive material it introduces some degree of deleterious mechanical loading. This can be estimated by considering the magnetostriction in terms of an equivalent force F_m acting on the sample. That is,

$$e = CH^2 = \frac{F_m}{A_m E_m} \tag{2.11}$$

where E_m is the Young's modulus of the sample. The relation between the unloaded (free) strain and the loaded strain, assuming that the fiber is perfectly bonded ($\eta = 1$) to the material, is given by:

$$e_{loaded} = \frac{e_{free}}{1 + A_f E_f / A_m E_m}. \tag{2.12}$$

Mechanical Resonance:

All magnetostrictive transducers exhibit mechanical resonance. The frequencies of these mechanical resonances depend on the geometry of the transducer, boundary conditions, and the effective mechanical modulus of the entire transducer (material, fiber, and adhesive). These mechanical resonances can be exploited to recover a significant portion of the response lost to demagnetization. In this thesis, two transducer designs are demonstrated and Chapter 4 will illustrate the effects of these constraints.

Equation 2.3 can now be modified to account for demagnetization, mechanical loading, and mechanical resonances as:

$$e = \frac{3\lambda_{sat}}{2H_A^2}\left[\frac{R(\omega)}{(1+A_f F_f / A_m E_m)(1+N\chi)^2}\right]H_{ext}^2 \qquad (2.13)$$

where R(ω) is the normalized response of the transducer as a function of frequency.

Based on the above analysis, it appears that the fiber with a magnetostrictive jacket would be least affected by demagnetization effects. This design also offers the possibility of mass production in long lengths, but depositing or sputtering a uniform coating with good mechanical and magnetic properties has been difficult. Packing presents an additional problem. In the amorphous wire transducer, a fiber is bonded to a 100 μm diameter wire having an iron-boron composition [2.2]. This geometry offers a favorable trade off between loading and demagnetization and can be produced in short lengths. The initial results have been encouraging but the magnetic response of these need to be better understood.

Magnetostrictive sensors, with fiber wrapped and bonded to rectangular strips and cylinders have demonstrated the best overall performance so far. We will review the results presented by these geometries with reference to nickel and metallic glass transducers.

The parameters of interest in characterizing magnetic field sensors and phase modulators are :

- minimum detectable magnetic field,
- linearity of response versus the applied magnetic field,
- directivity,
- frequency response, and
- noise constraints on performance.

As mentioned earlier, of the several magnetostrictive materials which can be used to strain the fiber in response to an external magnetic field, nickel [2.13, 2.14] and metallic glasses [2.15] have been the most commonly used. Metallic glass appeared to be the best suited for fiber sensor applications because

- of its availability in thin film strips,
- low cost,
- magnetic softness, as well as
- the possibility of varying the magneto-mechanical efficiency by annealing the sample [2.3].

Developments in fiber magnetometers utilizing metallic glasses included mainly the demonstration of:

- a large dynamic range,
- freedom from magnetic hysteresis, and
- long term stability with the use of a magnetic feedback nulling technique, [2.4]
- a minimum detectable field of 70 $fT/\sqrt{Hz}$ at a frequency [2.5] of approximately 34 kHz and of 3 $pT/\sqrt{Hz}$ at a low frequency [2.6] of 10 Hz, and
- a dc sensitivity [2.7] of 10^{-6} Oe per meter of fiber for a bandwidth of 1 Hz.

- multiplexing [2.8] of magnetometers utilizing the nonlinear relationship between the induced strain and the magnetic field,
- material studies on metallic glasses [2.9], and
- studies on detection schemes for improved signal analysis [2.10].

Such high detectabilities have been possible because of the long fiber interaction lengths [2.5, 2.11] of approximately 15 to 34 meters brought about by coiling the fiber on a multiple-layered metallic glass cylinder.

The increase in the induced phase shift with such long lengths of fiber is however reduced by:

- demagnetization effects [2.12] due to the multiple layers and the aspect ratio of the cylinder as compared to a flat strip configuration, and
- mechanical loading [2.1] because of the epoxy needed for attaching long lengths of fiber.

This thesis presents a new fiber optic magnetostrictive phase modulator and magnetometer utilizing the highly magnetostrictive rare-earth iron compound $Tb_xDy_{1-x}Fe_2$ (the trade name of which is Terfenol). This modulator and magnetometer demonstrated to have a high sensitivity, large dynamic range, good minimum field detectability, and a better structural suitability than metallic glasses.

Chapter 3 - Rare Earth Iron Laves Compounds for Magnetostriction

3.1 Introduction

The rare earth iron compounds (RFe_2, where R stands for Tb, Sm, Dy, Er, Tm) possess a large magnetocrystalline anisotropy, a large magnetostriction and high magnetic saturation. This makes these alloys potentially valuable for magnetostrictive transducers, permanent magnets, acoustic delay lines, and micropositioning devices of various kinds.

Along with the structural suitability of RFe_2 compounds for fiber optic implementations, the room temperature magnetostriction of these compounds is known to be about two orders of magnitude larger than metallic glass. This should provide a larger phase shifting coefficient, good minimum detectability, and a larger dynamic range, thus motivating us to study these compounds for applications in phase modulators and magnetometers. In this chapter we will study the properties of binary and pseudo-binary rare earth iron alloys and compounds.

Wallace and Skrabek [3.1] have shown that the rare earth moments couple antiferromagnetically to the iron moments in the RFe_2 compounds. Salmans, Strnat and Hoffer [3.2], in 1968, demonstrated that the RFe_2 compounds have the strongest exchange interactions and the highest ordering temperatures, with the least amount of magnetic transition metal. Thus the magnetostriction and anisotropic properties of the rare earth elements, having a large concentration of rare earth ions, were available at room temperature as opposed to cryogenic temperatures. Extensive magnetization measurements on a large number of RFe_2 binary and pseudo binary compounds were reported by Buschow and Von Stapele [3.3] and Burzo [3.4].

3.2 Magnetostriction of Binary Rare Earth Iron Alloys

The discovery of huge room temperature magnetostriction in the Tb-Fe compounds, particularly $TbFe_2$, kindled interest in the RFe_2 compounds. Figure 3.1 [3.5] shows the field dependence of the magnetostriction ($\lambda_{\parallel} - \lambda_{\perp}$ denotes the strain parallel to the magnetic field minus the strain perpendicular to the magnetic field) for the RFe_2 compounds. Outstanding among these compounds are $TbFe_2$ and $SmFe_2$ with room temperature magnetostrictions greater than 2000 ppm. This is attributed to the large magnetoelastic energy of the rare earth ion and the large rare earth iron exchange constant. The latter prevents the magnetostriction from falling from its low temperature value by maintaining the rare earth sublattice magnetization relatively intact at room temperature. A large magnetocrystalline anisotropy is indicated by the slow increase in magnetostriction with field. It can also be noted that the magnetostriction of $ErFe_2$,

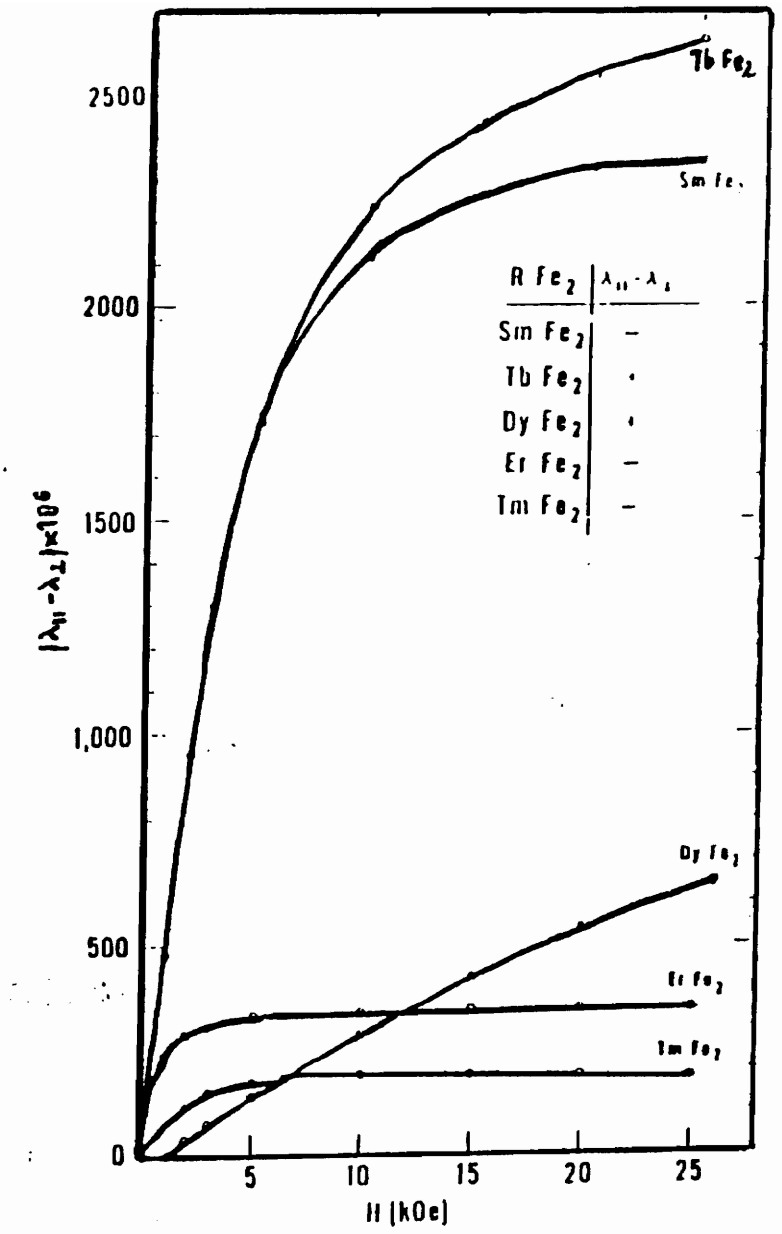

Figure 3.1. Field dependence of magnetostriction for the RFe_2 compounds [3.5].

$TmFe_2$ and to a lesser extent, $TbFe_2$ and $SmFe_2$, saturates at relatively low fields while that of $DyFe_2$ is far from saturation. The magnetostriction of some of the RFe_2 compounds is listed in Table 3.1. Some ternary compounds (Tb_xFe_{1-x} compounds) and other rare earth transition metal compounds are also included. For comparison, some transition metals and oxides are also included.

Table 3.1. Magnetostriction of some polycrystalline materials at room temperature [3.5].

Material	$10^6\lambda_s$	Material	$10^6\lambda_s$
Fe	- 9[b]	YFe_2	1.7
Ni	- 35[b]	$SmFe_2$	-1560
Co	- 62[b]	$Gd_{.3}Tb_{.7}Fe_2$	847
Sm, Tb, Dy	~ 0[c]	$TbFe_2$	1753
Fe_3O_4	40[d]	$TbFe_2$ (sputtered)	308
$CoFe_2O_4$	-110[d]	$Tb_{.8}Dy_{.2}Fe_2$	1330
$NiFe_2O_4$	- 26[d]	$Tb_{.3}Dy_{.7}Fe_2$	1068
$Y_3Fe_5O_{12}$	- 2[e]	$DyFe_2$	433
Tb_2Co_{17}	47	$ErFe_2$	- 229
YCo_3	0.4	$TmFe_2$	- 123
$TbCo_3$	65	$TbFe_{1.6}Co_{.4}$	995
Tb_2Ni_{17}	- 4	$TbFe_{1.6}Ni_{.4}$	730
		85% Tb - 15% Fe	539
		70% Tb - 30% Fe	1590
		$TbFe_3$	693
		Tb_2Fe_{17}	131

a. For the rare earth compounds, λ_s denotes $\frac{2}{3}(\lambda_{||} - \lambda_{\perp})$ at 25 kOe.

b. See R. M. Bozorth, Ferromagnetism (Van Nostrand, New York, 1951).

c. Non-magnetic at room temperature.

d. See J. Smit and H. P. Wijn, Ferrites, (Wiley, New York, 1959).

e. A. Clark, R. DeSavage, W. Coleman, E. Callen and H. Callen J. Appl. Phys. 34, 1296 (1963).

3.3 *Magnetic Anisotropy of RFe_2 Compounds*

Rare earths occupy sites of cubic symmetry, they possess a large magnetic anisotropy and magnetostriction. A potential application of a material with high cubic anisotropy and magnetic saturation at room temperature is as a permanent magnet. Figure 3.2 and Figure 3.3 show the magnetization versus temperature curves for $DyFe_2$ and $ErFe_2$. For $DyFe_2$ the easy axis of the crystal is [100] and for $ErFe_2$ the easy axis is [111]. For both, $DyFe_2$ and $ErFe_2$, we can see that even at 120 kOe, it is impossible to polycrystallize samples at 4°K. A list of anisotropy constants for some cubic materials is shown in Table 3.2.

Table 3.2. Anisotropy constants for some cubic materials [3.5].

Metal	$10^{-4}K_1$(ergs/cm^3)	Ferrite	$10^{-4}K_1$(ergs/cm^3)
Fe	45[a]	$Ga_{.44}Fe_{2.54}O_4$	- 81[d]
Ni	- 5[a]	$CoFe_2O_4$	260[e]
70% Fe-Co	- 43[b]	$Co_{.8}Fe_{2.2}O_4$	290[f]
65% Co-Ni	- 26[c]	$Co_{1.1}Fe_{1.9}O_4$	180[f]
$ErFe_2$	-330	$Co_{.3}Zn_{.2}Fe_{2.2}O_4$	150[f]
$DyFe_2$	2100		

a. U. Hoffman, Z. angew. Phys. 22, 106 (1967).
b. L. W. McKeehan, Phys. Rev. 51, 136 (1937).
c. J. W. Shih, Phys. Rev. 50, 376 (1936).
d. R. F. Pearson, J. Appl. Phys. 31, 1608 (1960).
e. R. Perthel, G. Elbinger, and W. Keileg, Phys. Status Solidi 11, 151 (1966).
f. R. M. Bozorth, E. F. Tilden, and A. J. Williams, Phys. Rev. 99, 1788 (1955).

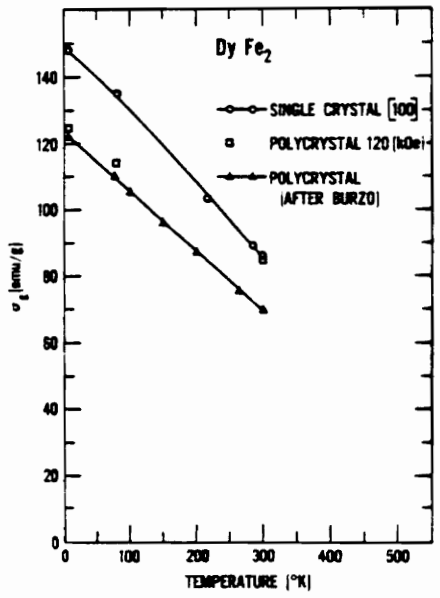

Figure 3.2. Magnetization versus temperature curves for $DyFe_2$ [3.5].

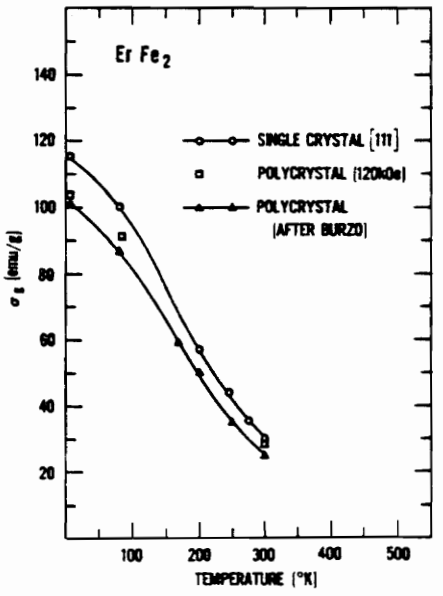

Figure 3.3. Magnetization versus temperature curves for $ErFe_2$ [3.5].

3.4 Magnetostriction of Pseudo binary Laves Phase Compounds

The figure of merit for magnetostrictive transducer applications is the ratio of the square of the magnetostriction to the anisotropy energy. Thus for magnetostrictive phase modulators and magnetometers, we require a material with a large magnetostriction and small anisotropy energy. Table 3.3 shows the signs of the magnetostriction λ, and the anisotropy constants k1 and k2 for the heavy RFe_2 compounds [3.5]. From the table, we observe that $TbFe_2$ and $DyFe_2$ have the same sign for magnetostriction. Also, the anisotropy constants k1 and k2 are of opposite signs in $TbFe_2$ and $DyFe_2$. This indicates that for the ternary compound $Tb_xDy_{1-x}Fe_2$, for some concentration x, the magnetostriction should be large and the magnetic anisotropy small. Figure 3.4 shows the room temperature measurements of $\lambda_{||} - \lambda_{\perp}$ as a function of x. We observe that the magnetostriction peaks at $x \sim 0.3$. This is because the magnetization is easily rotated for the fields employed. From table 3.1 we can see that the saturation magnetostriction for $Tb_xDy_{1-x}Fe_2$ is 1068 ppm at 25 kOe. This ternary compound thus has potential applications as a magnetostrictive transducer. It is commercially available under the trade name Terfenol. Other similar ternary systems with anisotropy minimums are $Tb_xHo_{1-x}Fe_2$, $Er_xYb_{1-x}Fe_2$, and $Tm_xYb_{1-x}Fe_2$. The anisotropy constants k1 and k2 can be minimized for a specific temperature in a suitably chosen ternary system.

Table 3.3. Polarity of magnetostriction and anisotropy constants [3.5].

	$TbFe_2$	$DyFe_2$	$HoFe_2$	$ErFe_2$	$TmFe_2$	$YbFe_2$
λ	+	+	+	-	-	-
K_1	-	+	+	-	-	+
K_2	+	-	+	-	+	-

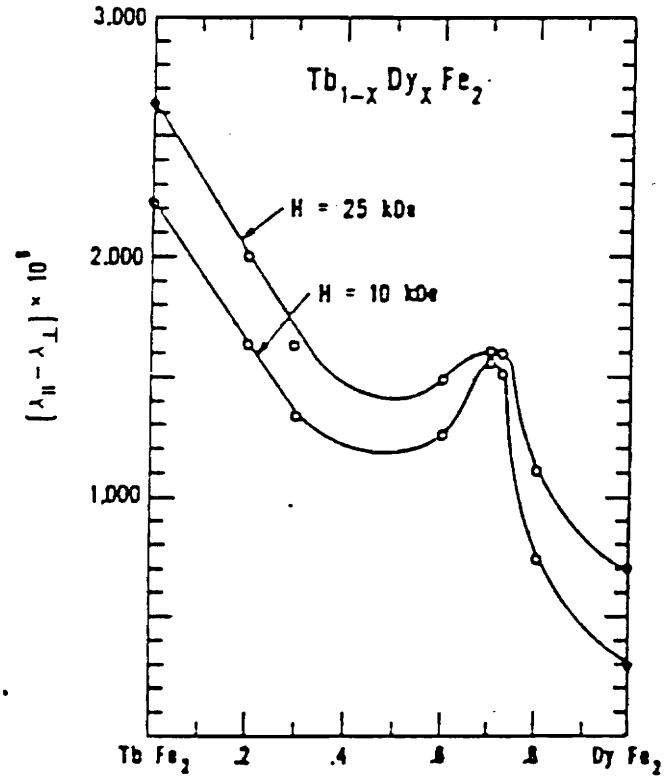

Figure 3.4. Magnetostriction of $Tb_{1-x}Dy_xFe_2$ as a function of x [3.5].

Thus, by selecting a suitable pseudo binary compound it is possible to adjust both the sign and the magnitude of the magnetostriction and anisotropy simultaneously. A compound with a large positive or negative magnetostriction and small anisotropy can be selected for magnetostrictive transducer applications or a compound with a large positive or negative anisotropy can be selected for permanent magnet materials.

3.5 Terfenol for fiber optic phase modulator and magnetometer.

In the preceding sections we have seen that the measured values of the magnetostrictive constant of RFe_2 compounds at room temperature far surpasses that of other materials. Outstanding among these compounds are $TbFe_2$ and $SmFe_2$, with magnetostriction greater than 2000 ppm. It is possible to further enhance this magnetostriction by utilizing in the construction of the sensor element a bimetallic strip composed of these and similar alloys [3.5]. It is known that the magnetostriction of the ternary compound $Tb_xDy_{1-x}Fe_2$ is a function of x, and peaks where x is approximately 0.3, indicating that the composition $Tb_{0.3}Dy_{0.7}Fe_2$ is optimized for large magnetostriction. The reported [2.1] magnetostrictive strain at saturation in a representative metallic glass samples is approximately 30 ppm for field strengths in excess of approximately 30 Oe. In comparison, the saturation value of 1068 ppm is achieved at approximately 25 kOe for Terfenol. Assuming linearity below approximately 2.5 kOe, and a value of 500 ppm at 1 kOe, the magnetostriction for $TbFe_2$ is about 5 ppm at 10 Oe. Although at present the magnetostriction of Terfenol appears to be less than that for metallic glasses for low amplitude fields of a few Oe, metallic glass would become saturated at very low field amplitudes of approximately 30 Oe, thus precluding its use for the detection of fields of larger magnitude, and limiting its dynamic range considerably. In comparison, the high saturation field of approximately 25 kOe for Terfenol increases its dynamic range of detection by an order of magnitude or more. This particular feature assumes a greater importance in a fiber magnetostrictive phase modulator where the phase shifting coefficient is of prime importance, as compared to the minimum field detectability which is of primary concern for sensing purposes. Thus one can apply a larger magnetic field in a

modulator application and utilize the large magnetostriction at high fields to derive extremely large phase shifts which cannot be achieved with the metallic glass transducers.

One of the main limitations of the metallic glass transducers has been the mechanical structure of the sensor element. The compliance of thin metallic glass films necessitates that several layers of the film be bonded together first with the fiber, and then bonded onto this cylindrical structure. In the absence of mechanical loading and the deleterious effects of demagnetization, a linear scaling of the phase shift is expected for a corresponding increase in the fiber interaction length. However, this situation represents an ideal case, and earlier reports have shown that such effects do limit the value of the effective magnetostrictive parameter [2.12]. In contrast, Terfenol is available in the form of a sturdy metallic rod (the dimensions of the sample are considered in the following chapter), so the effect of mechanical loading is negligible, leading to a linear scaling of the phase shift with the fiber length. Also, the geometry of the sensor head is of importance, and the effect of small bending radius on the intensity loss in the fiber and the birefringence of the fiber limits the smallest radius to which the metallic glass cylinder can be formed. This is particularly of importance in applications where a magnetic probe of extremely small dimensions is required by applications.

Chapter 4 - Experimental Arrangements, Results, and Discussion.

4.1 Interferometry

4.1.1 Introduction

Interferometric sensor designs offer the highest performance and the greatest flexibility of design. In this class of sensors the optical phase of light passing through the optical waveguide is modulated by the field to be detected. Then, by comparing the phase of light in the signal fiber to that in the reference fiber, this phase modulation is detected interferometrically. These sensors have a very low loss since the light remains in the fiber and is also very sensitive because the device uses the interference of light. In the next subsection we will discuss two beam interferometry with reference to the Mach Zehnder interferometer.

4.1.2 Two Beam Interferometry

The measurement of extremely small differential phase shifts generated by a measurand in an optical fiber is possible with two beam interferometry. The optical phase delay (in radians) of light passing through a fiber is given by [1.7]

$$\phi = nkL \tag{4.1}$$

where n is the refractive index of the fiber core, k is the optical wave number in vacuum ($2\pi/\lambda$, λ being the wavelength), and L the physical length of the fiber. The optical path length is referred to the quantity nL. By differentiating Equation 4.1, small variations in the phase delay can be found:

$$\frac{d\phi}{\phi} = \frac{dL}{L} + \frac{dn}{n} + \frac{dk}{k} \tag{4.2}$$

The first two terms describe the transduction mechanisms by which fibers can act as sensors. Changes in temperature, pressure, and magnetic field generally result in different contributions to $d\phi$ via the dL and dn terms. To produce dominant dL terms, most sensing mechanisms rely on some sort of material bonded to the fiber. However, due to the strain optic coefficient of the fiber, an accompanying dn occurs. The last term takes into account any wavelength variations of the laser source, and is useful in considering noise terms for some demodulation approaches [1.7].

A typical Mach Zehnder interferometer configuration is shown in Figure 2.1. A coherent single mode source is launched into one arm of the input coupler. The light is then split, nominally equally by a coupler, into the reference arm and the sensing arm, and recombined by the output coupler. An interference signal between the two beams is then formed which, after propagating the length of the output fiber, is detected by the photodetector(s). Let the power coupling coefficients of the two couplers be k_1 and k_2 and assume a certain optical loss α_s and α_r associated with the sensing and reference paths respectively. The optical fields at one output of the interferometer originating from the signal and reference arms are:

$$E_r = E_o\sqrt{\alpha_r k_1 k_2}\cos(\omega_o t + \phi_r) \tag{4.3}$$

and

$$E_s = E_o\sqrt{\alpha_s(1-k_1)(1-k_2)}\cos(\omega_o t + \phi_s). \tag{4.4}$$

The output intensity of the interferometer can be expressed as

$$I = \langle E_r^2\rangle + \langle E_s^2\rangle + 2\langle E_s E_r\rangle \tag{4.5}$$

where $\langle . \rangle$ denotes the time average over a period much longer than $2\pi/\omega$. The output intensity is given by:

$$I = I_o[\alpha_r k_1 k_2 + \alpha_s(1-k_1)(1-k_2) + 2\sqrt{\alpha_s\alpha_r k_1 k_2(1-k_1)(1-k_2)}\cos(\phi_r - \phi_s). \tag{4.6}$$

The output fringe visibility of the interferometer is given by the standard definition:

$$V = \frac{I_{max} - I_{min}}{I_{max} + I_{min}} \tag{4.7}$$

The complementary output of the interferometer is given by:

$$I' = I_o[\alpha_r k_1(1-k_2) + \alpha_s(1-k_1)k_2 + 2\sqrt{\alpha_s\alpha_r k_1 k_2(1-k_1)(1-k_2)}\cos(\phi_s - \phi_r). \tag{4.8}$$

For ease of mathematical evaluation, we will assume $\alpha_S = \alpha_T = \alpha$ and $k_1 = k_2 = 0.5$ and V=1 then,

$$I = \frac{I_o\alpha}{2}(1+\cos\Delta\phi) \tag{4.9}$$

and

$$I' = \frac{I_o\alpha}{2}(1-\cos\Delta\phi). \tag{4.10}$$

The differential phase shift in the interferometer is separated into a signal term $d\phi$ of amplitude ϕ_s and frequency ω and a slowly varying phase shift ϕ_d. Thus, for simplicity the interferometer outputs can be written as

$$I = \frac{I_o\alpha}{2}[1+\cos(\phi_d + \phi_s \sin\omega t] \tag{4.11}$$

and

$$I' = \frac{I_o\alpha}{2}[1-\cos(\phi_d + \phi_s \sin\omega t] \tag{4.12}$$

The photodetector converts these intensity outputs into electrical currents, and the differential combination of these outputs produces an output

$$i = \varepsilon I_o \alpha \cos(\phi_d + \phi_s \sin \omega t), \tag{4.13}$$

where ε is the responsivity of the photodetectors. Equation 4.13 can be expanded in terms of Bessel functions such that the output is of the form:

$$i = \varepsilon I_o \alpha \left\{ \cos\phi_d \left[J_o(\phi_s) + 2\sum_{n=1}^{\infty} J_{2n}(\phi_s) \cos 2n\omega t \right] + \sin\phi_d \left[2\sum_{n=0}^{\infty} J_{2n+1}(\phi_s) \sin((2n+1)\omega t) \right] \right\} \tag{4.14}$$

where $J_n(\phi_s)$ is the Bessel function of order n and argument ϕ_S.

As can be seen, it is a nontrivial task to retrieve the signal information $d\phi$ in the presence of a slowly varying ϕ_d. If we consider the form of Equation 4.14 for small arguments (i.e., $\phi_S << 1$), $J_0 = 1$ and $J_1(\phi_S) = \phi_S/2$, and considering only the time varying portion of equation 4.14, it may be simplified as

$$di \sim \varepsilon I_o \alpha \sin\phi_d \phi_s \sin \omega t \tag{4.15}$$

The amplitude of the signal $d\phi$ depends on the value of $\sin\phi_d$. When $\phi_d = m\pi$, the signal will vanish and when $\phi_d = (2m+1)\pi/2$, the signal is maximized. This is the so called "fading problem" of interferometric fiber sensors. For maximum phase modulation sensitivity and quasi-linear response to small phase changes a sensor system must be biased at its quadrature or Q point ($\phi_d = (2m+1)\pi/2$, where m is an integer). Again, this point gives a quasi-linear output for small phase changes. For larger changes, the output is cosinusoidal. Laser frequency fluctuations, changes in air temperature, polarization

fluctuations, vibrations of the lead in/out fibers are a few of the factors that can move the system away from the quadrature point.

For providing a linear output and eliminating drift and signal fading due to the problems mentioned above, a number of demodulating schemes have been demonstrated. The two most popular techniques can be broadly classified as homodyne detection and heterodyne detection. The most active homodyne technique involves actively stabilizing the interferometer at its Q point [2.13]. A feedback network controls a fiber wrapped piezo electric cylinder which is placed in one arm of the interferometer for phase modulation. However, switching transients causes problems in this system. The heterodyne techniques requires an optical frequency shifter and so is a relatively complicated technique.

Under the assumption that the signal being measured by the interferometric system is sinusoidal, and referring to Equation 4.16, where ω_s is the frequency of the signal phase shift, x is the modulation depth, and $\phi_o(t)$ is the random phase drift due to the noise sources listed above, a number of demodulation schemes are possible. These include the J_0(null), J_1(max), J_1(null), J_1/J_2, J_1/J_3 and the J1..J4 techniques [4.1]. If the modulation depth is much less than one, and quadrature is maintained, then $J_1(\phi_s)$ can be determined directly from the fundamental component and x can be obtained by inverting the Bessel function. If B is not known, one of the methods just mentioned above can be used. All but the J1..J4 technique requires that $\phi_d = 0$ and/or $\phi_d = \pi/2$ be maintained. The J1..J4 technique allows direct linear readout of dynamic phase shifts without system stabilization of phase biasing. The next section describes this technique.

4.2 J1..J4 Detection Technique

The J1..J4 method is a phase measurement technique which is applicable to optical interferometry in general for the measurement of dynamic sinusoidal displacements. It provides linear measurement of dynamic phase changes by using spectral analysis of the photodetector output in a no feedback, no phase bias interferometer [4.1].

Bessel functions $J_n(x)$ of the first kind [4.1], can be used to represent the instantaneous voltage at the output of the photodetector as

$$V(t) = A + B\left(\left\{J_o(x) + 2\sum_{n=1}^{\infty} J_{2n}(x)\cos\left[2n(\omega_s t + \phi_s)\right]\right\}\cos\phi_o(t) - \left\{2\sum_{n=1}^{\infty} J_{2n-1}(x)\sin\left[(2n-1)(\omega_s t + \phi_s)\right]\right\}\sin\phi_o t\right), \tag{4.16}$$

where A = 2ν and B = 2νb (with ν the voltage due to either of the fiber outputs and b is the interferometer mixing efficiency), x is the modulation depth, ω_S is the angular frequency of the signal phase, ϕ_S is a phase constant, and $\phi_O(t)$ is the random phase shift due to ambient temperature and pressure variations [1.7, 4.1]. Using the recurrence relationship between Bessel functions $J_n(x)$ of the first kind,

$$x = \frac{2iJ_i(x)}{J_{i-1}(x) + J_{i+1}(x)} \tag{4.17}$$

x can be determined without any phase bias as [4.2]

$$x^2 = \frac{4i(i+1)V_iV_{i+1}}{(V_i + V_{i+1})(V_{i-1} + V_{i+1})}, \tag{4.18}$$

where $i > 1$, $V_i = 2BGJ_i(x)$ is the voltage amplitude of the ith frequency component. By passing the interferometer output through a signal analyzer, this can be obtained easily. G = cos ϕ_0 or sin ϕ_0 for i even or odd respectively. For i = 2, this relationship can be explicitly written as

$$x^2 = \frac{V_2V_3}{(V_2 + V_4)(V_1 + V_3)}. \tag{4.19}$$

We can see that n and B as defined in Equation 4.16 are canceled. Also, the factors sin ϕ_0 or cos ϕ_0, which represent random phase drifts do not appear in the equation. This means that random phase drifts, polarization drifts, fringe contrast variations and intensity fluctuations of the laser all cancel out and need not be controlled. Thus, this technique can be implemented by simple bandpass filtering of V(t) at four successive peaks and performing the computation, or by using a spectrum analyzer.

The J1..J4 technique was used to measure the minimum detectable phase shift of the two sensor configurations described later. A large dynamic range with a minimum detectable phase shift of 0.1 radian is obtained.

4.3 Experimental Setup and Sensor Designs

4.3.1 Experimental Setup

An all-fiber Mach Zehnder interferometer was constructed utilizing two single mode optical fibers as shown in Figure 4.1. Light is injected into one arm of the input coupler using a semiconductor laser diode manufactured by Seastar Optics Inc. The operating wavelength of the laser is 1300 nm. The sensing arm, with the Terfenol sensor / modulator is placed inside a solenoid. The solenoid of length 10.2 cm and average diameter 5.89 cm, consisted of nine layers of 130 turns each, leading to a total of 1170 turns. The electrical resistance of the resulting coil was adjusted to allow 290 mA for a voltage of 20 Vp-p. The applied magnetic field strength H calculated was 36 Oe for an input voltage of 20 Vp-p. The reference arm and the rest of the fiber in the sensing arm, with the couplers was placed in a transparent pyrex box to prevent external perturbations from affecting the performance of the system.

The output from the photodetector was amplified and fed into a digital oscilloscope that performed a Fast Fourier Transform to provide the amplitudes at the fundamental frequency and its next three harmonics. These amplitudes were substituted into the Equation 4.18 to measure the phase shift by the J1..J4 method. As discussed earlier, this method provides a direct, linear and self-consistent readout of the dynamic phase change, independent of random phase drifts, source intensity fluctuations and fringe visibility change with polarization changes. This method was used directly to determine the nonlinear coefficients of the phase shift with respect to the input voltage to the solenoid. To characterize the frequency response of the sensor, the $J_1(\max)$ method was used.

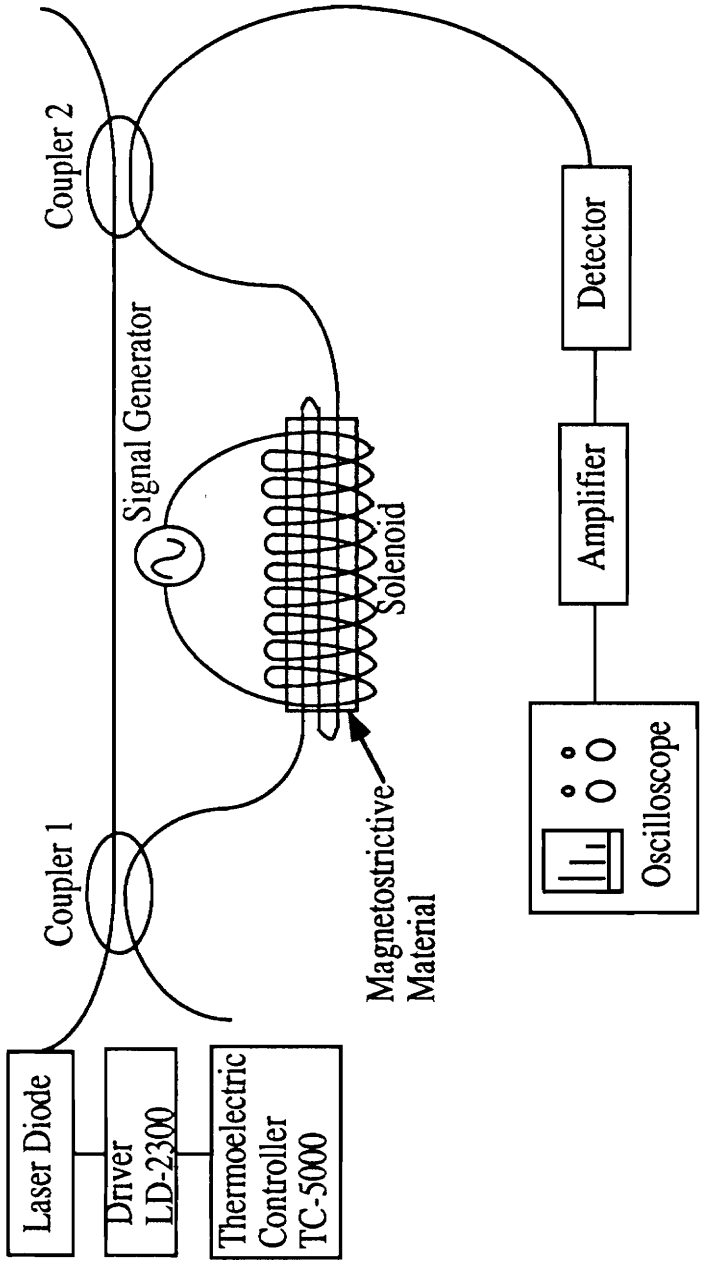

Figure 4.1: All-fiber Mach-Zehnder interferometer arrangement for the measurement of magnetic field and magneto-optical phase modulation.

4.3.2 Sensor Design # 1

A 72.6 cm section of fiber in one arm of the interferometer was bonded with a low modulus epoxy to a cylindrical Terfenol rod of length 36.3 mm and diameter 6.6 mm, as indicated in Figure 4.2(a). The fiber was oriented so it made twenty passes over the rod and covered much of the surface of the rod, except for the lower arc that was in contact with a metal support, as indicated in Figure 4.2(b). The rod and the metal support were placed within the solenoid, and the J_1(max) method was used to characterize the frequency response of the sensor. Then, the J1..J4 technique was used to determine the linearity of the response.

4.3.3 Sensor Design #2

In this approach the fiber was not bonded to the Terfenol rod. Instead two light weight plastic fixtures were made, as shown in Figure 4.3(a), and then bonded to the ends of the Terfenol sample with epoxy. Figure 4.3(b) shows the front view of the sensor. The fiber from the sensing arm of the interferometer was then wound around the structure, making seven passes around it. The interaction length of the fiber was 114.3 cm. This was then placed on a metal support inside the solenoid. Care was taken to adjust the height of the sensor inside the solenoid, so that it would be at the center of the coil.

4.4 Experimental Results and Discussion

4.4.1 Results of Sensor Design # 1

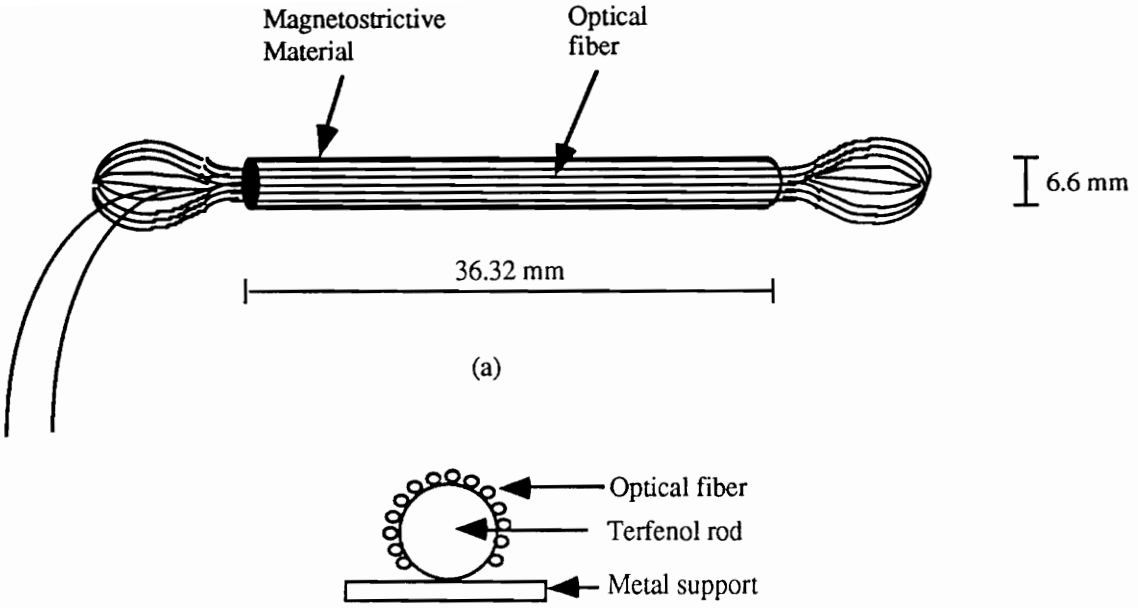

(b) Cross sectional view of (a).

Figure 4.2: Geometry of the sensor/modulator configuration with the fiber bonded onto the magnetostrictive rod.

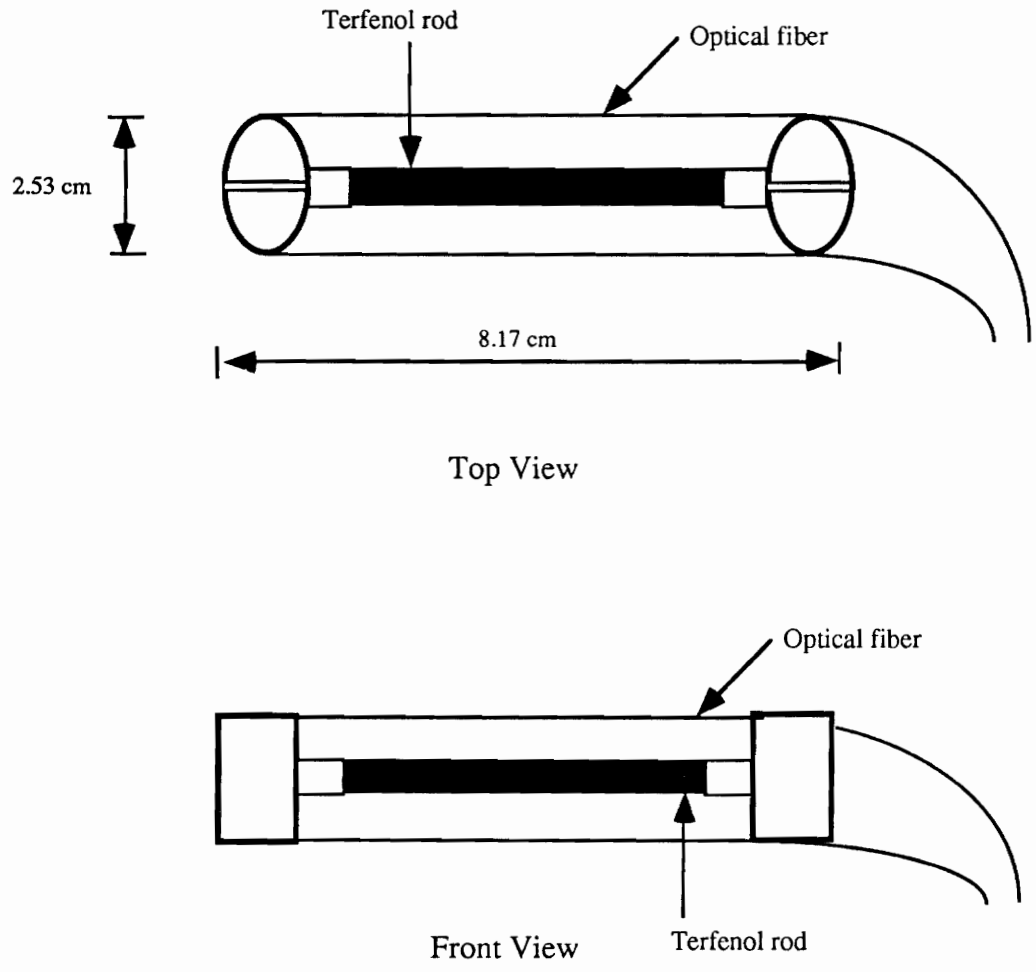

Figure 4.3: Geometry of the second sensor/modulator with the fiber wound around the Terfenol structure.

Figure 4.4 shows the phase shift measured by the J1..J4 method as a function of the input voltage to the solenoid at a frequency of 200 Hz. The frequency resolution of the spectrum analyzer was 4 Hz for the range of frequency chosen. The least squares fit to the third order for this plot was determined to be

$$\phi = 0.006\ v^3 - 0.115\ v^2 + 0.799\ v + 0.008, \qquad (4.20)$$

where ϕ is the phase shift, and v is the applied peak voltage. The linear phase shifting coefficient is calculated to be 1.102 rad/Vp-m, and the corresponding phase shift normalized to the magnetic field is 0.306 rad/G-m. A conversion factor of 3.6 G/Vp was utilized in arriving at this value.

The phase shifting coefficient (PSC) at near-dc frequencies was determined by applying a triangular waveform at approximately 0.2 Hz. Figure 4.5 shows the corresponding output of the interferometer as a function of time. The phase shift of π radians for an input voltage change of 9.22 V (peak to peak) corresponds to a PSC of 0.94 rad/Vp-m. It is thus clear that the PSC is larger by approximately 0.16 rad/Vp-m for the higher frequency of 200 Hz.

Figure 4.6 shows the frequency spectrum of the photodetector output for an input voltage of 0.2 Vp. Comparing the measured output voltage at 200 Hz to the noise floor at frequencies higher than 1 kHz, a minimum detectable phase shift of better than 1 μrad was obtained, which corresponds to 2 μG/m for a 4 Hz bandwidth and 1 $\mu G/\sqrt{Hz}$ per meter of interaction length of fiber. When a fiber interaction length of about 30 m is used, the

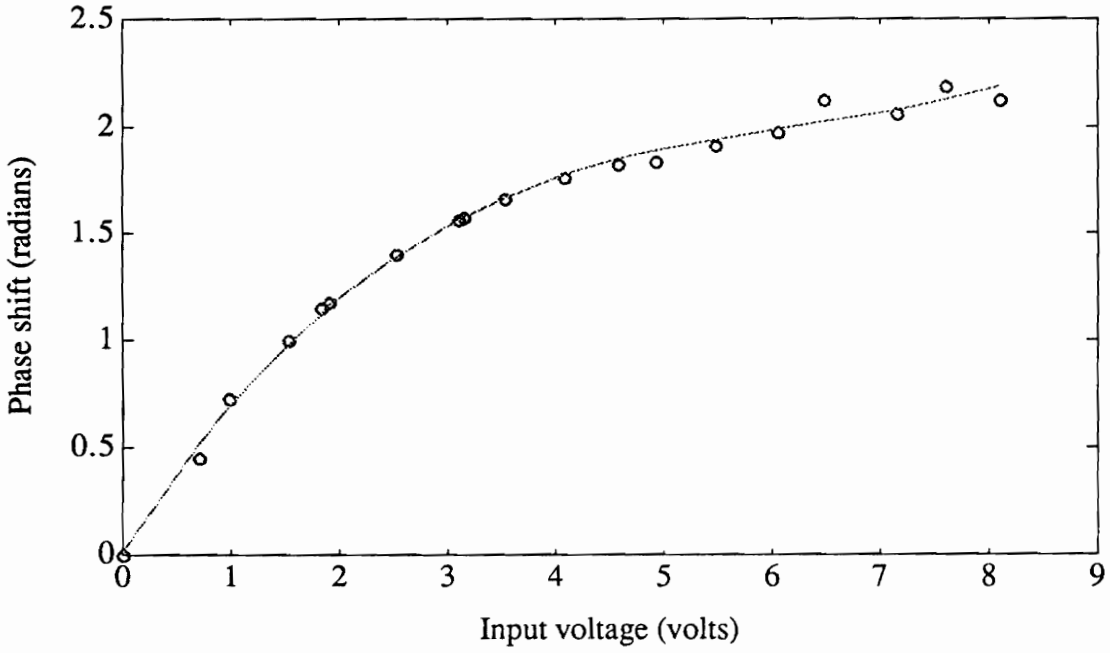

Figure 4.4: Phase shift as a function of the input voltage at a frequency of 200Hz

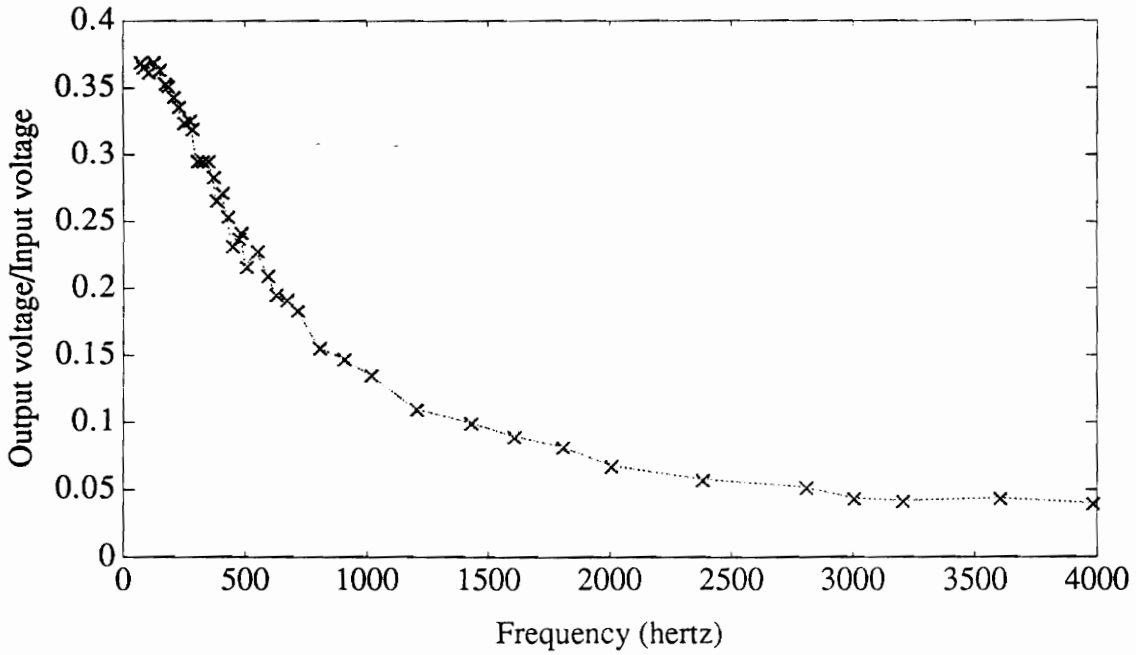

Figure 4.7: Frequency response of the first sensor configuration.

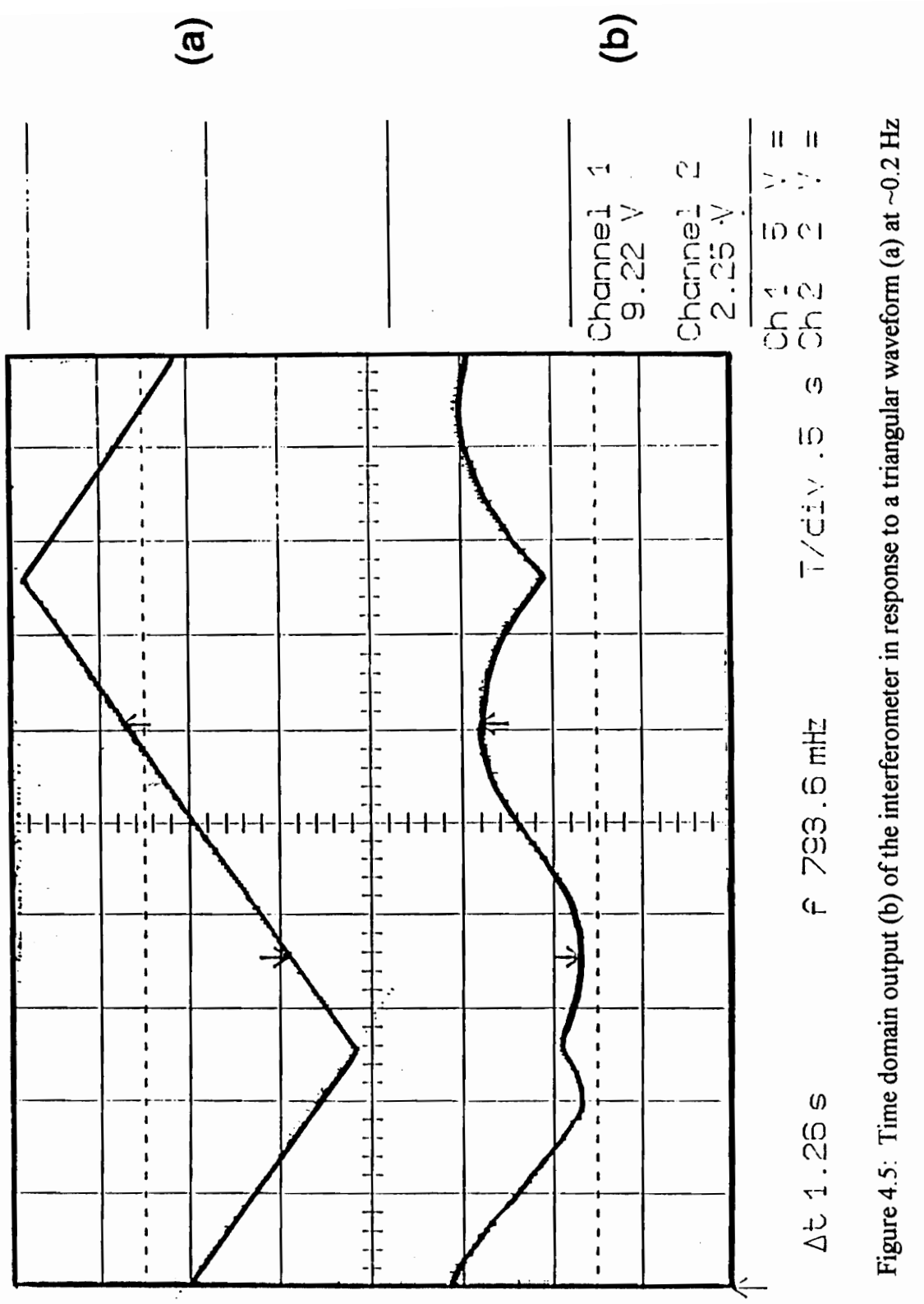

Figure 4.5: Time domain output (b) of the interferometer in response to a triangular waveform (a) at ~0.2 Hz

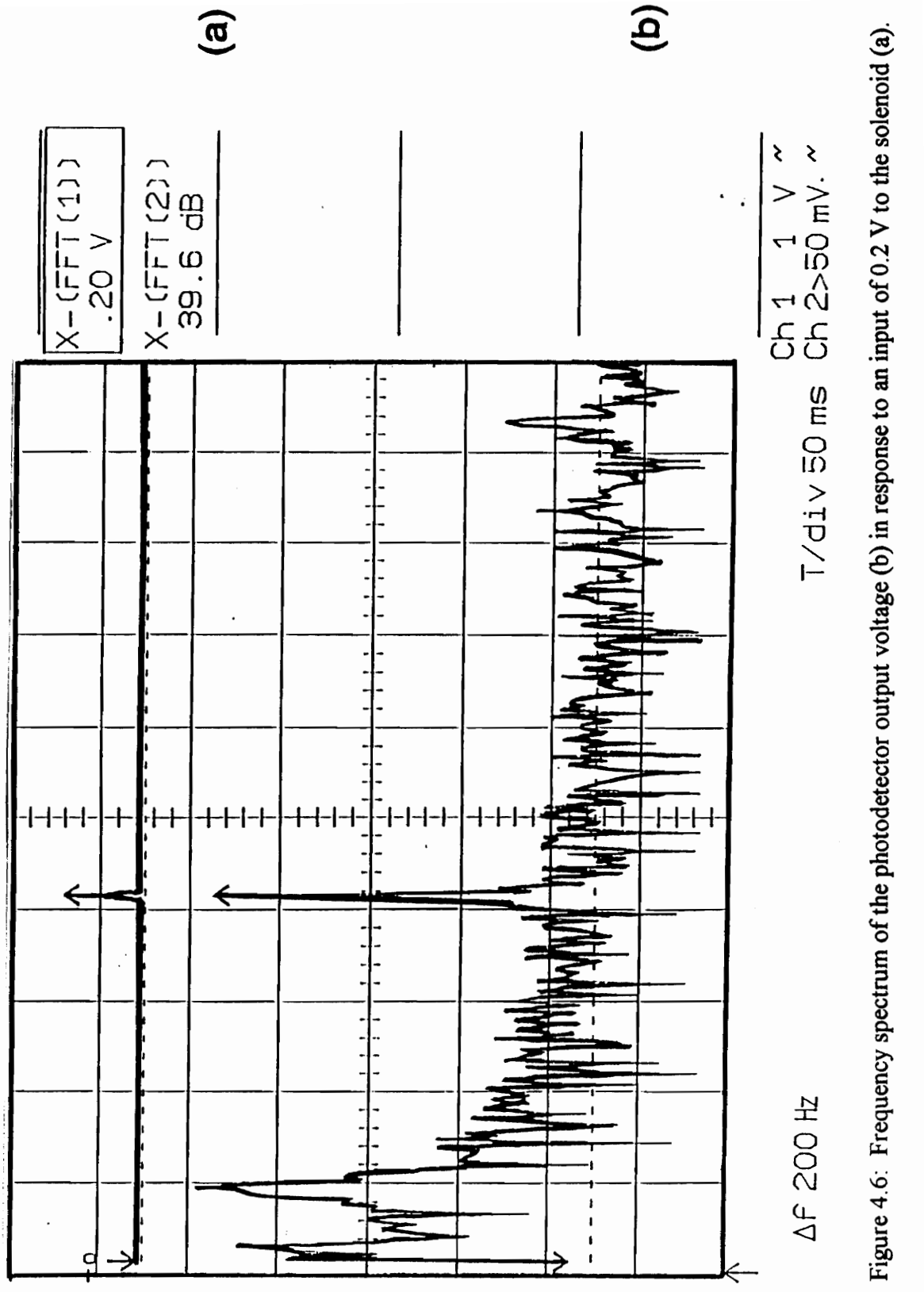

Figure 4.6: Frequency spectrum of the photodetector output voltage (b) in response to an input of 0.2 V to the solenoid (a).

projected minimum detectable magnetic field is seen to be 3 pT/$\sqrt{\text{Hz}}$. This is comparable to the best results that have been reported for this frequency range.

To characterize the frequency response of the sensor the J_1(max) detection technique, as described earlier, was used. Figure 4.7 shows the output normalized by the input plotted versus frequency. The input voltage at 200 Hz was 296 mV. We can see that the structure has a resonance peak around 60 Hz to 100 Hz. Thus, by operating the sensor at its resonance peak, the phase shifting coefficient will be scaled similarly.

To ensure the repeatability of measurements, the linearity of the response and the frequency response were verified. Figure 4.8 shows the phase shift as a function of the input voltage, redone at a frequency of 200 Hz. The least squares fit to the third order for this plot was determined to be

$$\phi = 0.006v^3 - 0.112v^2 + 0.777v - 0.014 \qquad (4.21)$$

where ϕ is the phase shift and v is the applied peak voltage, as described before. We can see that the curve fit is almost identical to the one obtained earlier. The linear phase shifting coefficient is calculated to be 0.95 rad/Vp-m and the corresponding phase shift normalized to the magnetic field is 0.2638 rad/G-m. Within the limits of experimental error, these results are similar.

Figure 4.9 shows the frequency response of the sensor. However, a higher input voltage of 761 mV at 200 Hz was used. From the figure we observe that we obtain a sharper

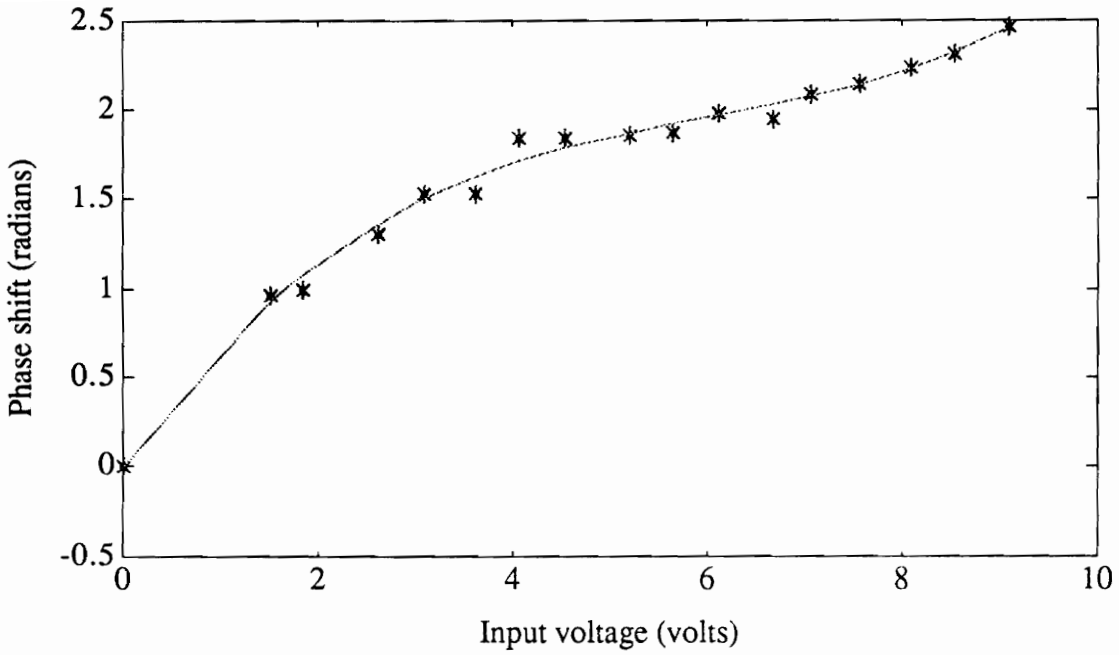

Figure 4.8: Phase shift as a function of the input voltage at a frequency of 200Hz.

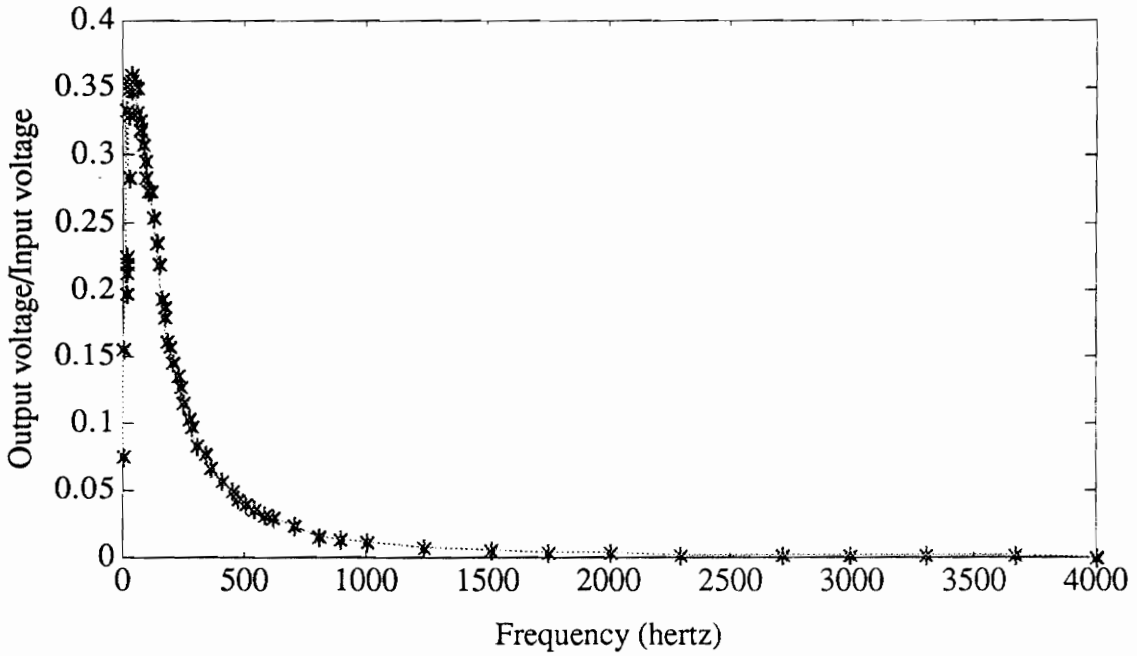

Figure 4.9: Frequency response of the first sensor configuration.

resonance peak but the basic shape of the frequency response is preserved. The resonance frequency in this case is around 50 Hz to 80 Hz.

4.4.2 Results of Sensor Design #2

The second configuration was made to reduce the effects of bonding the fiber with an adhesive to the magnetostrictive material. The aim was to increase the sensitivity and we hoped to shift the resonance frequencies to higher values.

Figure 4.10 shows the phase shift measured by the J1..J4 method as a function of the input voltage to the solenoid at a frequency of 200 Hz. The frequency resolution of the spectrum analyzer was 4 Hz for the range of frequency chosen. The least squares fit to the third order for this plot was determined to be

$$\phi = 0.008\ v^3 - 0.118\ v^2 + 0.638\ v + 0.0018 \qquad (4.22)$$

where ϕ is the phase shift, and v is the applied peak voltage. The linear phase shifting coefficient is calculated to be 0.49 rad/Vp-m, and the corresponding phase shift normalized to the magnetic field is 0.136 rad/G-m. A conversion factor of 3.6 G/Vp was utilized in arriving at this value.

To characterize the frequency response of the sensor the $J_1(max)$ detection technique, as described earlier, was used. Figure 4.11 shows the output normalized by the input plotted versus frequency. The input voltage at 200 Hz was 852 mV. We observe that we have

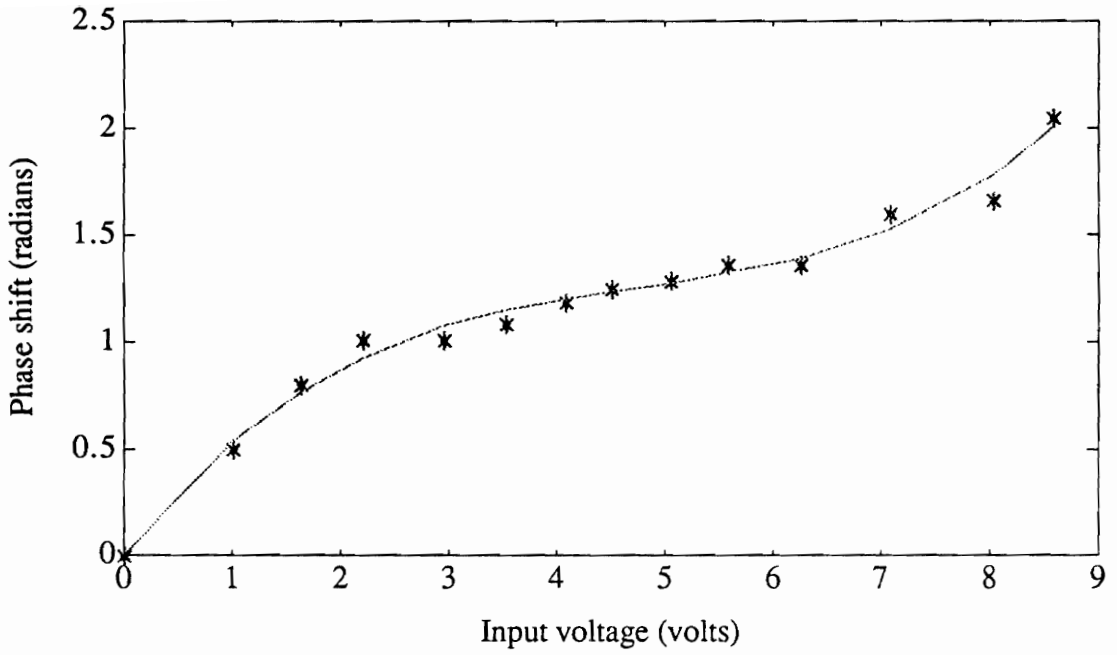

Figure 4.10: Phase shift as a function of the input voltage at a frequency of 200Hz

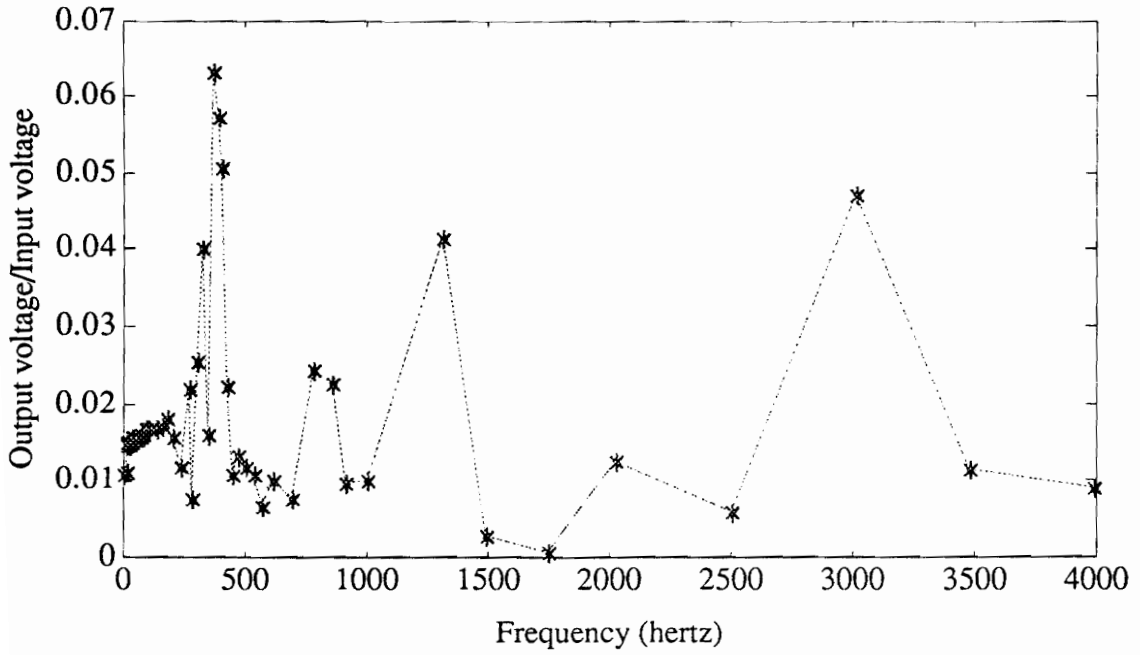

Figure 4.11: Frequency response of the second sensor configuration.

been successful in moving the resonance peaks to higher frequencies. This sensor configuration exhibits resonance at 322 Hz, 368 Hz, 780 Hz, 1305 Hz, and 3010 Hz. We should note that the phase shift was measured at a frequency of 200 Hz. At this frequency the output voltage was 13.3 mV. Considering the resonance peak at 3010 Hz, the output was 64 mV. Thus, by operating the sensor at one of its resonance peaks, the phase shifting coefficient will be increased. The ratio of the outputs at 3010 Hz and 200 Hz is five. Therefore, we can expect the phase shifting coefficient to increase by at least a factor of three. This would give us a projected phase shifting coefficient of approximately 1.47 rad/Vp-m. These, results would then be better than the first configuration.

To ensure the repeatability of measurements, the linearity of the response and the frequency response were verified. However, we noted that some turns of the fiber had come loose. Therefore, the fiber was rewound around the sensor structure. Thus, the tension with which the fiber was wound will be different. This should be considered while evaluating the results. Figure 4.12 shows the phase shift as a function of the input voltage, redone at a frequency of 200 Hz. The least squares fit to the third order for this plot was determined to be

$$\phi = 0.005v^3 - 0.071v^2 + 0.421v - 0.1, \qquad (4.23)$$

where ϕ is the phase shift and v is the applied peak voltage, as described before. We can see that the curve fit is similar to the one obtained earlier. The linear phase shifting coefficient is calculated to be 0.38 rad/Vp-m and the corresponding phase shift normalized to the magnetic field is 0.106 rad/G-m. Within the limits of experimental

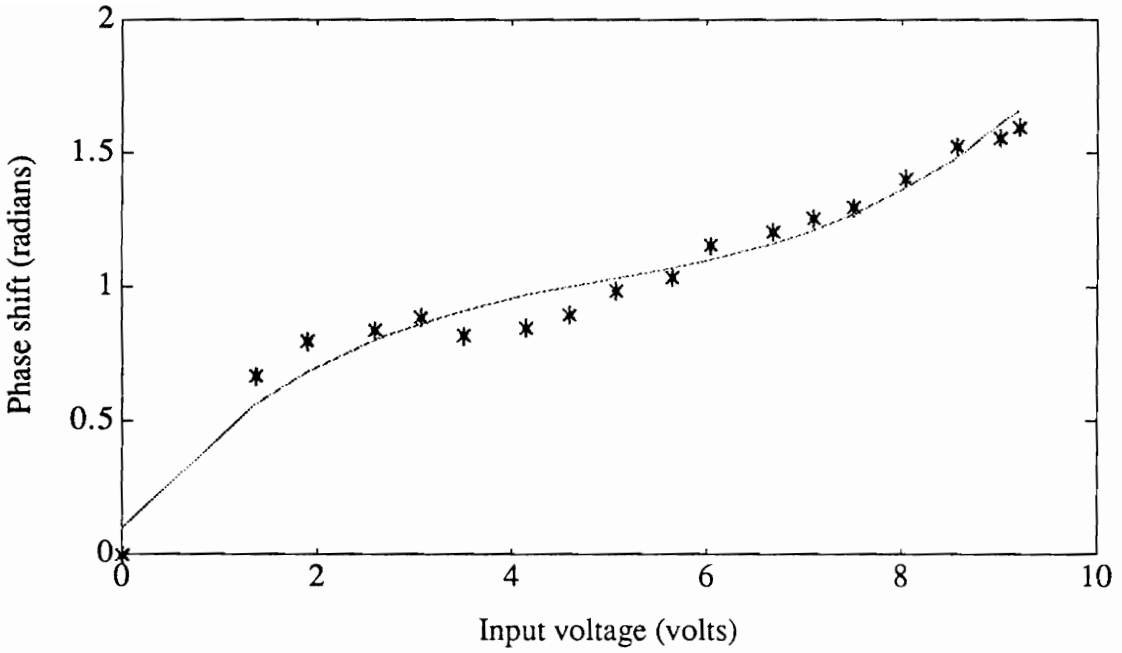

Figure 4.12: Phase shift as a function of the input voltage at a frequency of 200Hz

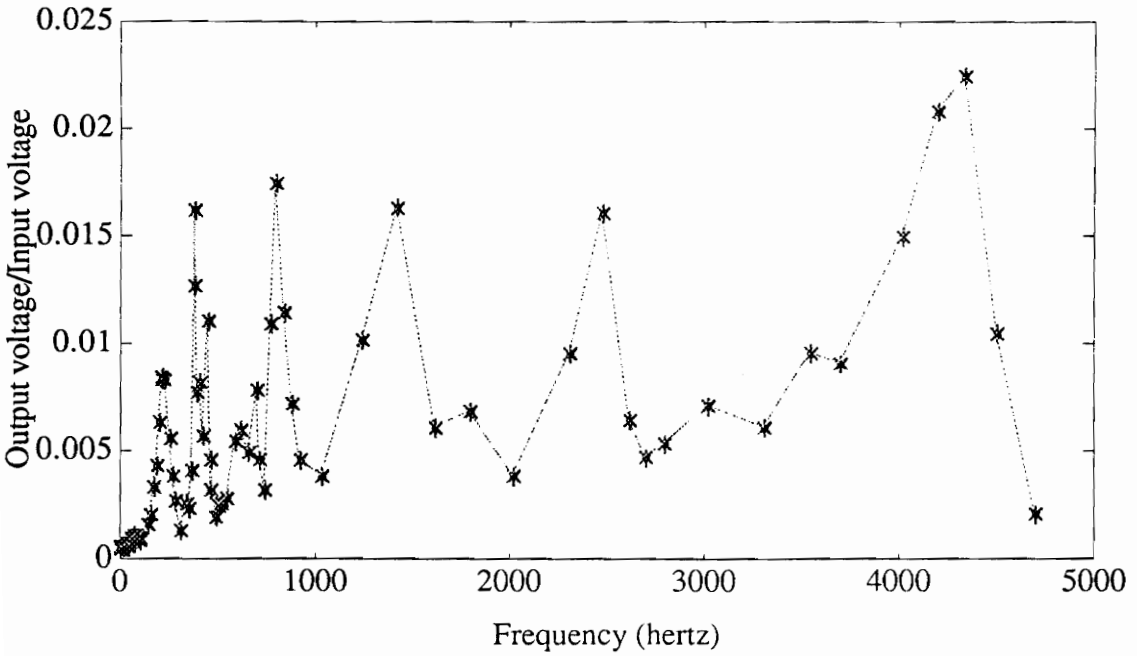

Figure 4.13: Frequency response of the second sensor configuration.

error, and the fact that the tension will be different than before, these results are in good accordance with each other.

Figure 4.13 shows the frequency response of the sensor. A higher input voltage of 990 mV at 200 Hz was used. We observe that we have been successful again in moving the resonance peaks to higher frequencies. This sensor configuration exhibits resonance at 379 Hz, 792 Hz, 1410 Hz, 2470 Hz, and 4340 Hz. Comparing these resonance frequencies with those obtained earlier, we observe that the results are similar to each other.

The projection of the minimum detectable magnetic field to longer lengths from the experimental values for shorter lengths is well within reason as the mechanical strength of the Terfenol rod is high enough to overcome the effects of loading by the long lengths of fiber. Such a linear projection would appear unreasonable in the case of compliant films of material, such as thin metallic glass strips or piezofilm strips which appear more prone to mechanical loading effects.

Chapter 5 - Conclusion and Future Direction

5.1 Conclusion

The experimental results presented have clearly demonstrated the utility of the Terfenol-based magnetostrictive fiber optic phase modulator and magnetometer. Large improvements in performance are possible with the inclusion of

- better signal detection schemes,
- a sensing element shape design that would allow larger fiber interaction length without extra unused lengths of fiber between multiple passes, and
- magnetic treatment (annealing) of the sample to optimize the sensitivity.

It must be stressed that the improvement in state-of-the-art technology is an ongoing process, and progress in achieving better values for the minimum detectability depends on the development of each of several contributing factors. Earlier reports have shown that better insights into material behavior are possible with fiber interferometry than conventional methods. To the best of our knowledge, the magnetic and magnetoelastic

properties of Terfenol have been studied only for very high field magnitudes, such as beyond a few hundreds of Oe. It is foreseen that a study of several properties at low fields would thus greatly facilitate the present understanding of the material phenomena. Further, the high accuracy and resolution possible with fiber interferometry would be positive factors, even for the study of similar material properties under high applied fields. It must be noted that reports on the magnetostrictive properties of materials have commonly used as a standard, resistive strain gages that leave much to be desired in performance in comparison to fiber optic methods.

5.2 Future Direction

It must be noted that the system configuration utilized for these measurements was kept to the minimum level of sophistication. Improvements in the minimum detectable field are possible with the utilization of

- a scheme in which the output from two detectors placed out of optical phase by 180^{o} leads to source intensity noise reduction, and
- feedback to the interferometer through a phase modulator to compensate for low frequency noise from random phase drifts.

Additionally, by employing magnetic shielding for these tests a contribution by ambient magnetic noise can be reduced. A mumetal shield could be used in future experiments, specially when low frequency fields are being measured. To increase the ac sensitivity a dc bias can be applied to the sensor. This can be achieved by using two concentric solenoids and applying a dc bias to one and using a known ac signal to the other coil. As

mentioned earlier, a sensing element shape design that would allow larger fiber interaction length without extra unused lengths of fiber between multiple passes, and magnetic treatment (annealing) of the sample to optimize the sensitivity, would certainly yield better figures of merit. Another interesting area to look into is to try and sputter Terfenol onto optical fiber, and then use this fiber with the magnetostrictive jacket in different sensor configurations. This will require sophisticated sputtering equipment.

References

1.1 W. B. Jones, Introduction to Optical Fiber Communication Systems, Holt, Rinehart, and Winston, Inc., New York, 1988.

1.2 F. R. Trowbridge and R. L. Phillips, "Metallic-glass fiber-optic phase modulators," Opt.Lett., vol. 6, pp. 636, 1981.

1.3 A.Yariv and H. V. Winsor, 'Proposal for detection of magnetic fields through magnetostrictive perturbation of optical fibers," Opt.Lett., vol. 5, pp. 87-89, 1980.

1.4 A. Dandridge, A. B. Tveten, G. H. Sigel, Jr., E. J. West, and T. G. Giallorenzi, Electron.Lett., vol. 6, pp. 636-, 1980.

1.5 K. P. Koo and G. H. Sigel, Jr., "Characteristics of fiber-optic magnetic-field sensors employing metallic glasses," Opt.Lett., vol. 7, pp. 334-336, 1982.

1.6 J. E. Lenz, C. D. Anderson, and L. K. Strandjord, "Magnetic materials characterization using a fiber optic magnetometer," J.Appl.Phys., vol. 57, pp. 3820-3822, 1985.

1.7 Ed. Eric Udd, "Fiber optic sensors: An introduction for engineers and scientists," John Wiley & Sons, Inc., 1991.

2.1 F. Bucholtz, K. P. Koo, G. H. Sigel, Jr., and A. Dandridge, "Optimization of the fiber/metallic glass bond in fiber-optic magnetic sensors," J.Lightwave Technol. LT-3, pp. 814-817, 1985.

2.2 K. P. Koo, F. Bucholtz, D.M.Dagenais, and A. Dandridge, "A compact fiber-optic magnetometer employing an amorphous metal wire transducer," IEEE Photonics Technol. Lett., vol. 1, pp. 464-466, 1990.

2.3 G. E. Fish, "Soft magnetic materials," Proc. IEEE, vol. 78, pp. 947-972, 1990.

2.4 K. P. Koo, A. Dandridge, F. Bucholtz, and A. B. Tveten, "An analysis of a fiber optic magnetometer with magnetic feedback," J.Lightwave Technol. LT-5, pp. 1680-1685, 1987.

2.5 F. Bucholtz, D. M. Dagenais, and K. P. Koo, "High-frequency fibre-optic magnetometer with 70 ft/$\sqrt{\text{Hz}}$," Electron. Lett., vol. 25, pp. 1719-1720, 1989.

2.6 D. M. Dagenais, F. Bucholtz, K. P. Koo, and A. Dandridge, "Demonstration of $3pT/\sqrt{Hz}$ at 10 Hz in a fibre-optic magnetometer," Electronics Lett., vol. 24, pp. 1422-1423, 1988.

2.7 K. P. Koo, A. Dandridge, A. B. Tveten, and G. H. Sigel, Jr., "A fiber-optic dc magnetometer," J. Lightwave Technol., vol. 1, pp. 524-525, 1983.

2.8 F. Bucholtz, A. D. Kersey, and A. Dandridge, J. Lightwave Technol., vol. 7, pp. 514, 1989.

2.9 M. D. Mermelstein and A. Dandridge, "Directional characteristics of field-annealed magnetoelastic amorphous metal magnetometers," J.Appl.Phys., vol. 61, pp. 1793-1794, 1987.

2.10 D. M. Dagenais, F. Bucholtz, K. P. Koo, and A. Dandridge, "Detection of low-frequency magnetic signals in a magnetostrictive fiber-optic sensor with supressed residual signal," J.Lightwave Technol., vol 7, pp. 881-886, 1989.

2.11 F. Bucholtz, A. M. Yurek,K. P. Koo, and A. Dandridge, "Low frequency, submicrogauss fibre-optic magnetometer," Electron.Lett., vol. 23, pp. 985-987, 1987.

2.12 F. Bucholtz, K. P. Koo, A. M. Yurek, J. A. McVicker, and A. Dandridge, "Preparation of amorphous metallic glass transducers for use in fiber optic magnetic sensors," J. Appl. Phys., vol. 61, pp. 3790-3792, 1987.

2.13 T.G.Giallorenzi, et al.,"Optical fiber sensor technology," IEEE J.Quantum Electron. QE-18, pp. 620-665, 1982.

2.14 V.S.Sudarshanam, "Multimode fibre axial strain sensor utilizing end reflection interference," J.Mod.Opt., vol. 39, pp. 615-624, 1992.

2.15 F.Bucholtz, D.M.Dagenais, K.P.Koo, and S.Vohra, "Recent developments in fiber optic magnetostrictive sensors," Proc. SPIE., vol. 1367, pp. 226-235, 1990.

3.1 W. E. Wallace and A. E. Skrabek, Rare Earth Research II; edited by Vorres, pp 431, 1964

3.2 L. R. Salmans, K. Strnat, and G. I. Hoffer, AIP Handbook, McGraw Hill, pp. 5-149, 1972.

3.3 K. H. J. Buschow, and R. P. Van Stapele, J. Appl. Phy., vol. 41, pp. 4066, 1970.

3.4 E. Burzo, Z. Agnew, Physik, vol. 32, pp. 127, 1971.

3.5 A. E. Clark, "Magnetic and magnetoelastic properties of highly magnetostrictive rare earth-iron laves phase compounds," Proc.AIP Conf. Magnetism and Magnetic materials-1973, No.18, Part 2, Ed.C.D.Graham, Jr., and J.J.Rhyne (AIP, New York, 1974), pp. 1015-1029.

4.1 V.S.Sudarshanam and K.Srinivasan, "Linear readout of dynamic phase change in a fiber-optic homodyne interferometer," Opt.Lett., vol. 14, pp. 140-142, 1989.

Vita

Ketan D. Kamdar was born in the city of Bombay, India, on January 20, 1970. In 1987 he graduated from the Chauhan Institute of Science, Bombay and was accepted into Bombay University's Electronics engineering program. In May, 1991 he received a Bachelor of Engineering degree in Electronics Engineering from Bombay University and enrolled in Virginia Polytechnic Institute and State University's Graduate School program in Electrical Engineering. While pursuing a graduate degree, Mr. Kamdar was employed by the Fiber and Electro-Optics Research Center. He completed his Master of Science degree in Electrical Engineering during May, 1993.

His professional interests include optical fiber sensing and communication technology, system theory, and applications of optoelectronic devices to personal communication systems. He is a member of the Optical Society of America, and Institute of Electrical and Electronics Engineers.